Report

Current Biology

Graded BMP signals modulate yellow and red color in fishes, impacting adult pigment patterns and conspecific shoaling behavior

Graphical abstract

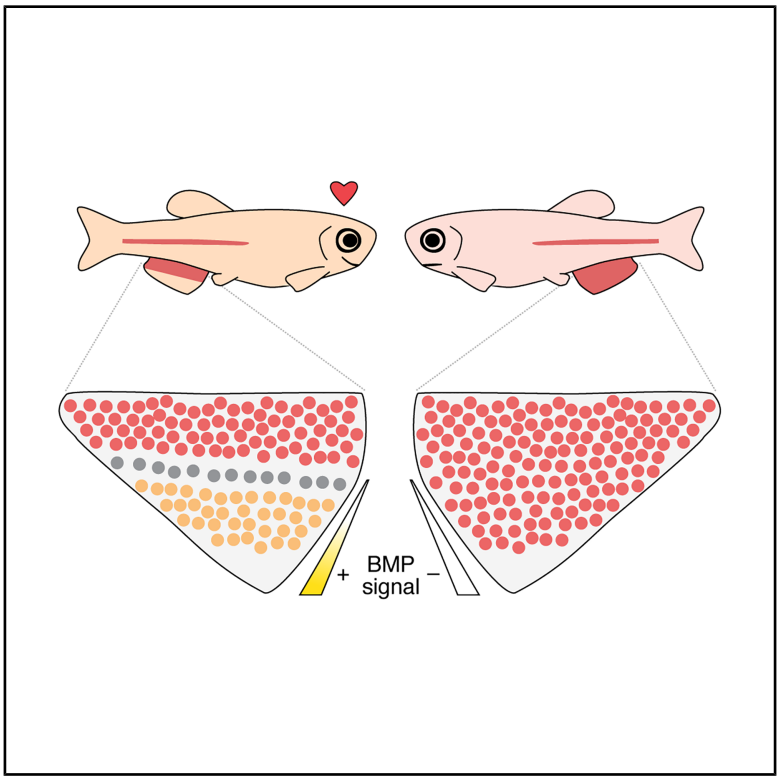

Authors

Delai Huang, Pietro L.H. de Mello, Tiffany Liu, ..., Jianguo Lu, Joseph C. Corbo, David M. Parichy

Correspondence

dparichy@virginia.edu

In brief

BMP signals a pattern of red vs. yellow pigment cells along fish fins with concentration-dependent thresholds for cell fate. Mutations that shift this balance alter color patterns and impact female shoalmate preference, linking a morphogen gradient to social behavior.

Highlights

- Thresholds of graded BMP signals specify red or yellow pigment cells in fins
- Higher BMP signaling drives xanthophores over erythrophores
- BMP mutants are super-red and preferred as shoalmates by females
- BMP-dependent pigment patterning is conserved in zebrafish and white cloud minnow

Huang et al., 2026, Current Biology *36*, 1–10
April 20, 2026
https://doi.org/10.1016/j.cub.2026.03.007

CellPress

Current Biology

CellPress
OPEN ACCESS

Report

Graded BMP signals modulate yellow and red color in fishes, impacting adult pigment patterns and conspecific shoaling behavior

Delai Huang,[1,6] Pietro L.H. de Mello,[1] Tiffany Liu,[1] Yu Liu,[2] Emaan H. Kapadia,[1] Yipeng Liang,[1] Jianguo Lu,[3,4] Joseph C. Corbo,[2] and David M. Parichy[1,5,7,*]

[1]Department of Biology, University of Virginia, 409 McCormick Road, Charlottesville, VA 22903, USA
[2]Department of Pathology and Immunology, Washington University School of Medicine, 660 South Euclid Avenue, St Louis, MO 63110, USA
[3]School of Marine Sciences, Sun Yat-Sen University, Zhuhai Campus, Haiqin Building No. 3, Zhuhai 519082, China
[4]Southern Marine Science and Engineering Guangdong Laboratory, Zhuhai Campus, Haiqin Building No. 3, Zhuhai 511458, China
[5]Department of Cell Biology, University of Virginia, 409 McCormick Road, Charlottesville, VA 22903, USA
[6]Present address: College of Animal Sciences, Zhejiang University, 866 Yuhangtang Road, Hangzhou 310058, China
[7]Lead contact
*Correspondence: dparichy@virginia.edu
https://doi.org/10.1016/j.cub.2026.03.007

SUMMARY

Among the most interesting adult traits are those with roles in animal communication. Yet, developmental mechanisms by which genes drive cell behaviors in building the final forms of such traits are rarely known. In this context, pigmentation is useful because colors and patterns often provide signals in mate choice, predation avoidance, and other behaviors,[1–3] and pigmentation is unusually accessible to observation and manipulation.[4,5] Here, we focus on some of the most prominent signaling colors—red, orange, and yellow—and show how BMP signaling at the cellular level allows for a very different kind of signal at the organismal level. Using pearl danio, *Danio albolineatus*,[6] we find that spatially and temporally graded BMP signals promote the development of yellow/orange xanthophores over red erythrophores in the fin of this species and a distantly related minnow, *Tanichthys albonubes*, and that conserved mechanisms, involving BMP co-receptor Rgmb, regulate the differentiation of other pigment cell types in corresponding locations of zebrafish, *D. rerio*. We further use mutants of *D. albolineatus* with more red or more yellow cells than the wild type to demonstrate female responsiveness to carotenoid-based color differences between males in shoaling preference assays. Our findings illustrate a chain of functions spanning hierarchical levels and provide a deeper understanding of pigmentary form and function and its evolution.

RESULTS AND DISCUSSION

A wide variety of morphological features are adapted for signaling between individuals: the peacock's ornate plumage that handicaps survival and so tells of underlying genetic quality, the enlarged claws of fiddler crabs that attract females and threaten rivals, and the antlers of male deer that indicate dominance and can be used to demonstrate social status when needed. The ethological context of such signals is often understood.[7,8] Occasionally, segregating alleles that modulate signal production are known. But how gene activities—from fixed alleles and segregating variants—are translated through morphogenesis and differentiation of cells into particular morphological outcomes remains largely mysterious, despite the importance of such information for understanding diversity of form and function in the natural world.

Among the many roles for integumentary pigmentation, signaling is especially common and important.[1,2,9] Yellow, orange, and red colors often function in mate choice and warning coloration and frequently depend on carotenoids that are dietarily acquired but endogenously processed.[3,10,11] In ectothermic vertebrates, specialized chromatophores of the neural crest lineage concentrate and display these pigments: red erythrophores and yellow-to-orange xanthophores.[12] To uncover molecular and cellular bases for the development and arrangements of these cells, we focused on minnows of the family Cyprinidae, which have diverse colors and color patterns, and, in the genus *Danio*, a phylogenetic proximity to zebrafish that makes them convenient for mechanistic and behavioral studies.[6,13,14]

To identify factors responsible for color and pattern, we reasoned that genetic pathways required for differentiating erythrophores and xanthophores from a common progenitor[15] could still be evident in the transcriptomes of fully pigmented cells. In pearl danio, *D. albolineatus*, xanthophores and erythrophores are intermingled on the body yet segregated to discrete regions in the fin, with erythrophores proximally, xanthophores further distally, and a region devoid of either cell yet containing black melanophores, at the distal tip[16] (Figures 1A and 1B). This pattern occurs in both sexes, though color differences are most pronounced in males,[15] which we used for all mechanistic analyses in this study. We isolated erythrophores and

Please cite this article in press as: Huang et al., Graded BMP signals modulate yellow and red color in fishes, impacting adult pigment patterns and conspecific shoaling behavior, Current Biology (2026), https://doi.org/10.1016/j.cub.2026.03.007

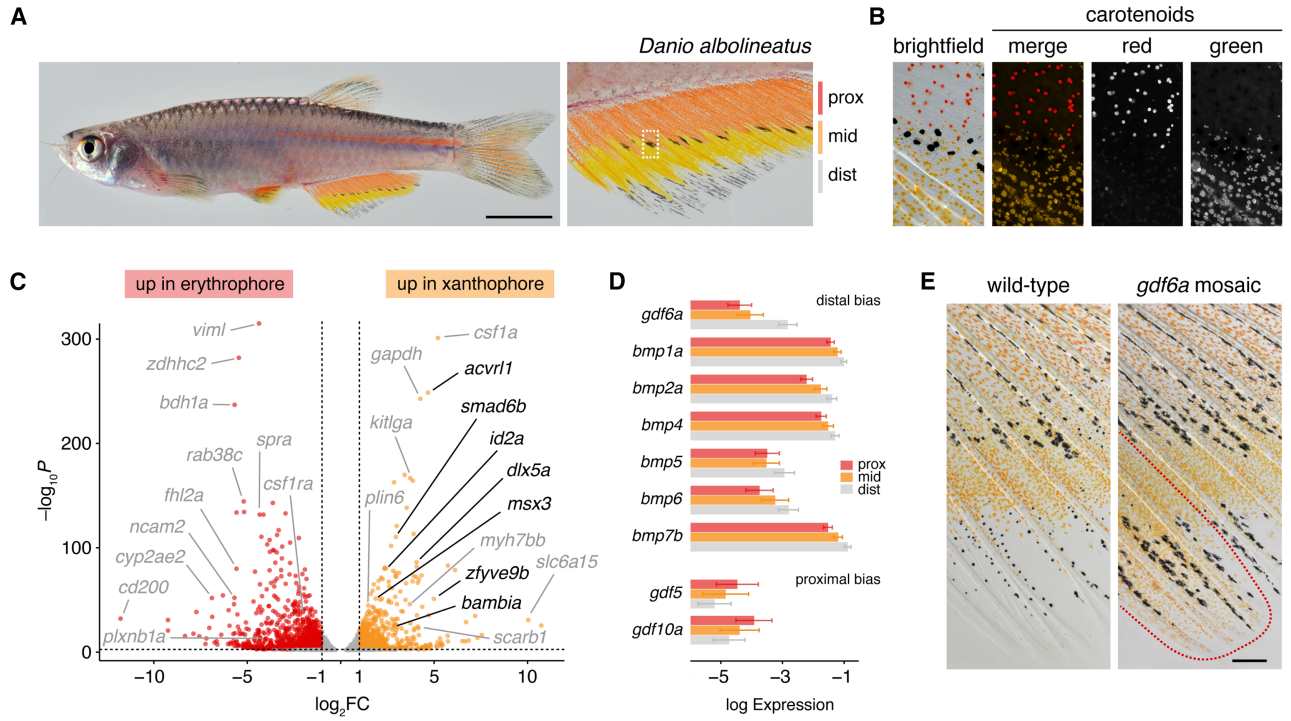

Figure 1. Pattern domains of erythrophores and xanthophores depend on BMP signals

(A) Wild-type male *D. albolineatus* with red erythrophores and yellow/orange xanthophores, intermingled on the body but spatially separated into proximal and middle regions in the fin. A few melanophores occur where erythrophores and xanthophores meet, and also distally near the fin tip. All figures illustrate male *D. albolineatus* unless otherwise indicated.

(B) Boxed region in A after contracting carotenoid vesicles toward cell centers with epinephrine. Red carotenoids of erythrophores autofluorescence in the red channel, whereas yellow/orange carotenoids of xanthophores autofluorescence in the green channel, here pseudocolored orange.

(C) Several BMP signaling or response genes were expressed more highly in xanthophores than erythrophores (shown in black). Additional genes with documented pigmentary functions, potential impacts on morphogenesis, or possible utility as markers due to expression differences are in gray. In xanthophores, more abundantly expressed genes included *scarb1* and *plin6*, required for the cellular uptake of carotenoids and concentration of carotenoids in lipid-containing vesicles,[17,18] respectively. By contrast, erythrophores expressed higher levels of *bdh1a* and *cyp2ae2*, which encode enzymes required to convert yellow carotenoids to red carotenoids.[11,15] See Data S1A–S1C.

(D) Transcripts of several BMP ligand genes were biased distally in their abundance (shown are model-predicted log mean expression ± 95% confidence intervals after controlling for cell-type-specific variation; see Data S1E).

(E) Mosaic loss-of-function for *gdf6a* expanded territories occupied by xanthophores toward the distal fin margin. Clones of cells extend proximodistally in fins,[15,19] and the dotted line here indicates the location of *gdfd6a*−/− cells, with distally localized xanthophores among melanophores, similar to the intermingling of xanthophores and melanophores on the body.[20,21]

Scale bars, 5 (A) and 250 μm (E).

See also Figure S1 and Data S1A–S1G.

xanthophores by dissecting corresponding regions of fins and then sorting for fluorescence of the transgenic reporter *aox5:nucEos*.[15] Comparison by bulk RNA sequencing revealed several transcripts associated with BMP signaling at markedly higher levels in xanthophores than erythrophores (Figure 1C; Data S1A) and enrichment for BMP pathway gene expression in xanthophores overall (Fisher's exact test, $p = 0.005$; Data S1B and S1C).

BMPs are well-known morphogens,[22–24] driving different cellular responses at different levels of signal strength and duration while also exhibiting their own context-specific activities.[25–28] BMPs also function in the outgrowth and regeneration of fins.[29,30] We therefore hypothesized that spatially or temporally graded BMP signals specify xanthophore vs. erythrophore fates. If so, genes encoding BMP or related ligands might be expressed differentially along the fin proximodistal axis, a prediction borne out by transcriptomic comparisons of single cells in the tissue environment (Figures S1A–S1C; Data S1D). Seven BMP ligand genes were expressed at higher levels in the distal fin compared with middle or proximal regions (Data S1E-1), with graded differences evident for 6 of these genes (Figures 1D and S1D; Data S1E–2). *gdf5* and *gdf10a* had proximal biases, and products of orthologous loci antagonize BMP2 and BMP4 signaling.[31,32] BMP ligand genes were expressed by basal epidermal cells, dermal fibroblasts and osteoblasts, and progenitors (Figure S1D).

To determine if xanthophores, erythrophores, or their progenitors are competent to receive BMP signals, we assayed expression of receptors by single-cell RNA sequencing at an earlier stage when pigmentary phenotypes were being acquired. These analyses revealed several BMP receptor genes—some expressed differentially between cell types—as well as modules of gene

Please cite this article in press as: Huang et al., Graded BMP signals modulate yellow and red color in fishes, impacting adult pigment patterns and conspecific shoaling behavior, Current Biology (2026), https://doi.org/10.1016/j.cub.2026.03.007

CellPress
OPEN ACCESS

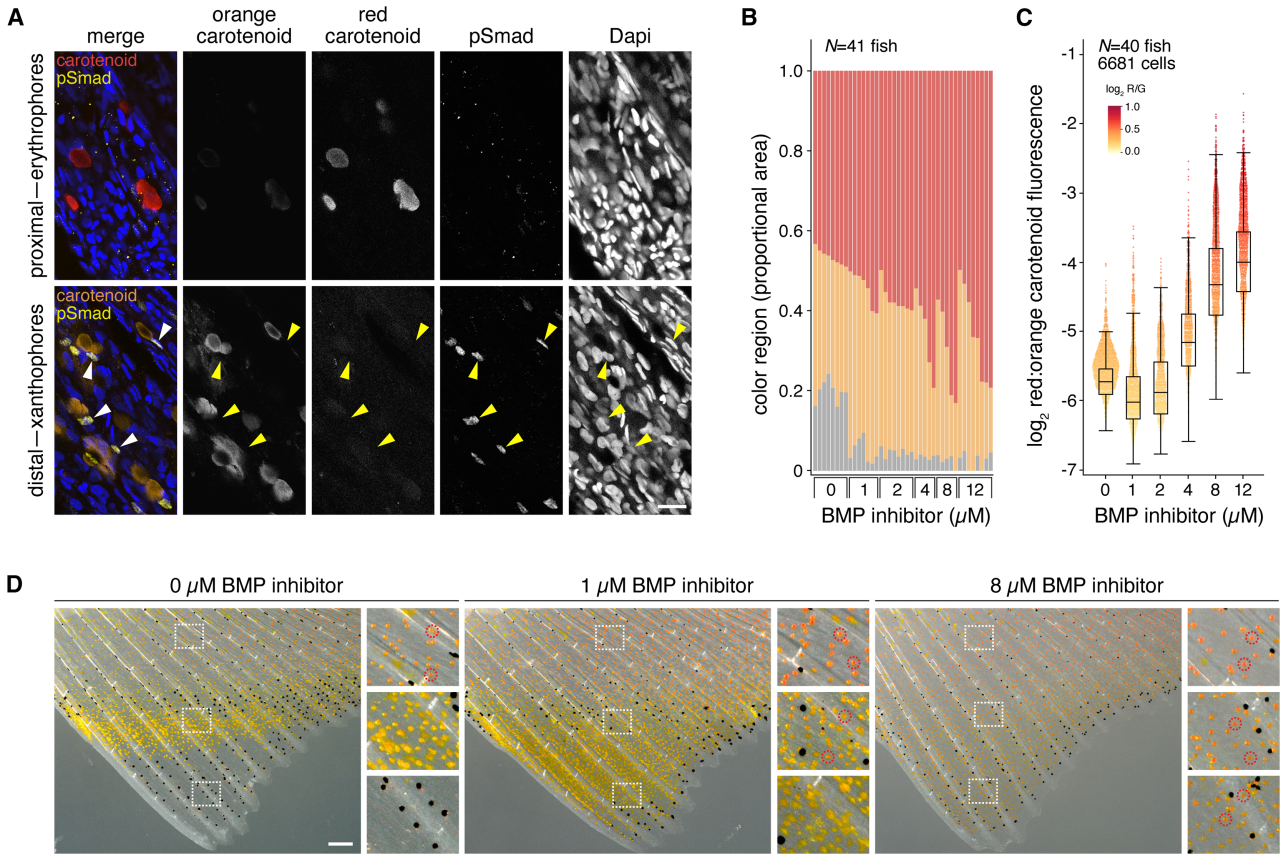

Figure 2. BMP signals specify xanthophores over erythrophores

(A) pSmad immunoreactivity was not evident proximally, where erythrophores are located, but was detected distally in nuclei of xanthophores. Different channels for the detection of cell-type-specific pigments are pseudocolored to match cell appearance in bright field (red ketocarotenoids of erythrophores detected in red and shown in red, and yellow carotenoids of xanthophores detected in green and shown in orange). Staining for pSmad (yellow in merge) coincided with locations of DAPI-stained nuclei and was adjacent to accumulations of pigment vesicles mobilized toward cell centers by epinephrine treatment.[15]

(B) Higher proportions of fins were covered by erythrophores than xanthophores upon treatment with BMP inhibitor. Each bar represents a single individual, ordered within treatments by extent of red coverage and showing distal regions without either cell type in gray.

(C) BMP inhibition also shifted ratios of red to yellow/orange carotenoids across cells measured individually for autofluorescence signatures (as in A). For each group, the box shows the interquartile range (IQR) with the median, and bars indicate 1.5 × IQR, superimposed on values for individual cells.

(D) Representative fins showing increasingly distal positioning of erythrophores and xanthophores with BMP inhibition. A few of the many example erythrophores, with red pigments, are circled in insets.

Scale bars, 20 (A) and 200 μm (D).

See also Figures S2–S4.

expression associated with xanthophore and erythrophore differentiation (Figures S1E–S1H; Data S1F and S1G). Compared with xanthophores, early erythrophores also expressed higher levels of the BMP inhibitor gene *fstl1b* (Figure S1E), whereas later erythrophores expressed higher levels of *fstl1b* and *fstb* ($\log_2$FC = 1.2 and 1.5, $q \leq$ 1.7E−6; Data S1A), suggesting diminished BMP signal reception may accompany differentiation.

Transcriptomic analyses thus pointed to differential BMP gene expression in the tissue environment, the competency of xanthophores and progenitors to receive such signals, and inhibitory factors potentially attenuating signals to erythrophores. As a first step in testing roles for BMP signaling, we targeted *gdf6a*, which functions in other pigmentary contexts.[33,34] Fish genetically mosaic for CRISPR-Cas9-induced mutations survived to post-embryonic stages and developed xanthophores along the distal fin margin where these cells are normally absent (Figure 1E).

Changes in xanthophore distributions in *gdf6a* mosaics, along with anatomical and temporal changes in BMP pathway gene expression, suggested that different levels of BMP signaling might be experienced by erythrophores and xanthophores. Indeed, erythrophores exhibited little to no detectable pathway activity, as inferred by immunohistochemical staining for pSmad, whereas xanthophores exhibited high levels of activity (Figure 2A). A distal bias of anti-pSmad immunoreactivity was evident after cell-type-specific colors had developed; proximo-distal variation was not evident among earlier-stage progenitors of nearly uniform color (Figure S2).

These observations suggested a model for chromatophore patterning during fin outgrowth[15] in which low BMP signals permit erythrophore differentiation proximally, higher levels induce xanthophore differentiation in middle-to-distal regions, and the highest levels prevent xanthophores from differentiating

Please cite this article in press as: Huang et al., Graded BMP signals modulate yellow and red color in fishes, impacting adult pigment patterns and conspecific shoaling behavior, Current Biology (2026), https://doi.org/10.1016/j.cub.2026.03.007

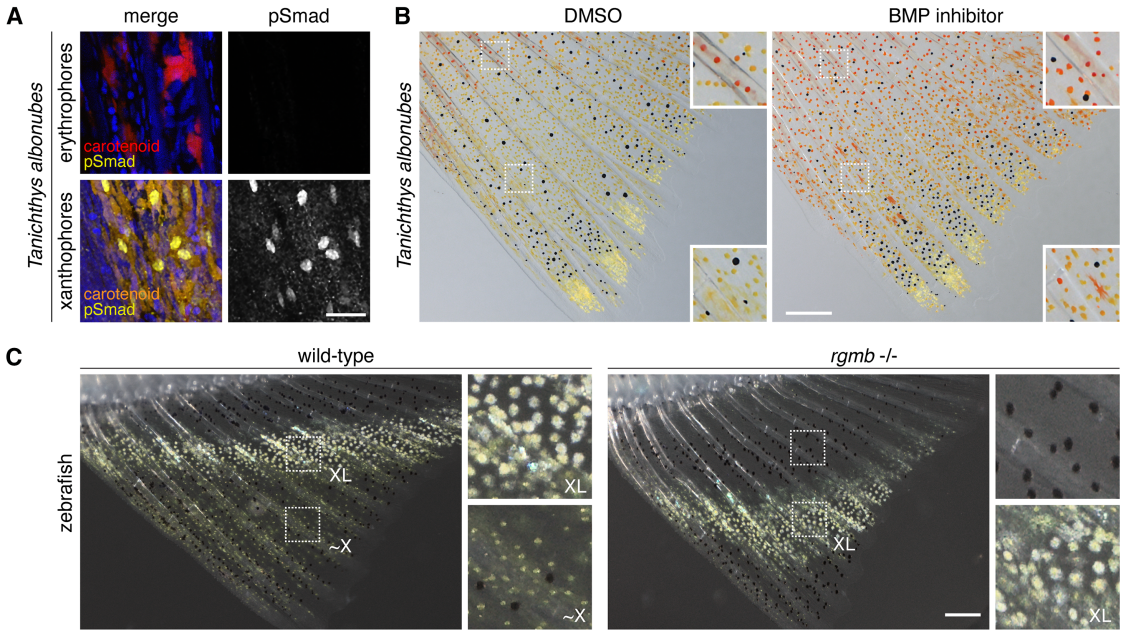

Figure 3. Conserved BMP signaling in pigment cell specification and pattern formation of other species

(A) *Tanichthys albonubes* erythrophores were pSmad−, whereas xanthophores were strongly pSmad+. Cytoplasmic signals in xanthophores were from pigment autofluorescence.

(B) BMP inhibition led to an expanded domain of erythrophores and a distal shift of xanthophores.

(C) Zebrafish early adult fin pattern with a light stripe of xantholeucophores (XL) and more distal xanthophore-like (~X) cells that are progenitors of XL.[40,41] In the *rgmb* mutant, defective for BMP signaling, XL were displaced distally, with melanophores occupying their normal location.

Scale bars, 20 (A) and 200 μm (B and C).

See also Figure S4.

at the distal tip. To test this idea, we inhibited BMP signaling during fin outgrowth beginning just prior to erythrophore and xanthophore differentiation using BMP type I receptor antagonist LDN-193189[35,36] (Figure S3A). Increasing doses led to increased areas covered by erythrophores, which extended further toward the fin tip, and increased redness within cells, assayed by fluorescence of red vs. yellow/orange carotenoids[15] (Figures 2B–2D). Distal limits of xanthophore regions shifted toward fin tips; at low doses, areas covered by xanthophores tended to be greater than in controls, and at high doses, these areas were more variable than in controls (Figure S3B).

These outcomes were consistent with flattening a signaling gradient: regions permissive for xanthophore development could be smaller or larger than controls, depending on the efficacy of inhibition across individuals and whether levels of signal fell within thresholds for xanthophore differentiation. Changes in pattern reflected alterations in locations and fates of cells differentiating from progenitors, rather than death, migration, or transdifferentiation of cells present at the start of treatments (Figures S3C and S3D). Though inhibitor treatment eliminated melanophores between erythrophore and xanthophore regions, melanophores did not themselves affect the other chromatophores: fin stripe melanophores developed only after the erythrophore-xanthophore boundary was established,[15,16] xanthophores extended distally into regions occupied by melanophores in *gdf6a*−/− mosaics (Figure 1E), and a mutant[37] that lacks anal fin melanophores developed an otherwise normal pattern (Figure S4A).

Roles for BMP signaling in patterning adult pigment cells were intriguing, so we asked whether they might be generalizable. To determine if BMP requirements for specifying xanthophores over erythrophores are conserved evolutionarily, we examined the white cloud minnow, *Tanichthys albonubes*, a distant relative of *Danio* within Cyprinidae,[38] with both types of cells. Xanthophores but not erythrophores exhibited strong pSmad immunoreactivity, as in *D. albolineatus* (Figure 3A). BMP inhibition likewise caused normally proximal erythrophores to differentiate across the fin, with xanthophores confined to distalmost regions (Figure 3B). A reciprocal shift was evident on the body, manifested in a dorsal shift in positions of a light "interstripe" of yellowish iridophores[39] and erythrophores and the upper boundary to a dark stripe of melanophores and blue iridophores (Figure S4B).

To test dependencies of other pigment cell types and patterns on BMP signaling, we turned to zebrafish. Unlike many danios, zebrafish lack erythrophores.[15] The anal fin pattern consists of dark stripes of melanophores and light interstripes of whitish-yellow xantholeucophores that develop through a xanthophore-like state[40,41] (Figure 3C). During pattern formation, relatively mature proximal xantholeucophores had low levels of pSmad immunostaining, whereas more distal xanthophore-like cells had strong pSmad staining (Figure S4C). By comparison to wild type, mutants for the non-canonical BMP co-receptor Rgmb[36,42] had reduced pSmad staining and a distal shift of mature xantholeucophores as the pattern was forming (Figure 3C). At later stages, proximal fin melanophores were positioned more distally,

Please cite this article in press as: Huang et al., Graded BMP signals modulate yellow and red color in fishes, impacting adult pigment patterns and conspecific shoaling behavior, Current Biology (2026), https://doi.org/10.1016/j.cub.2026.03.007

CellPress
OPEN ACCESS

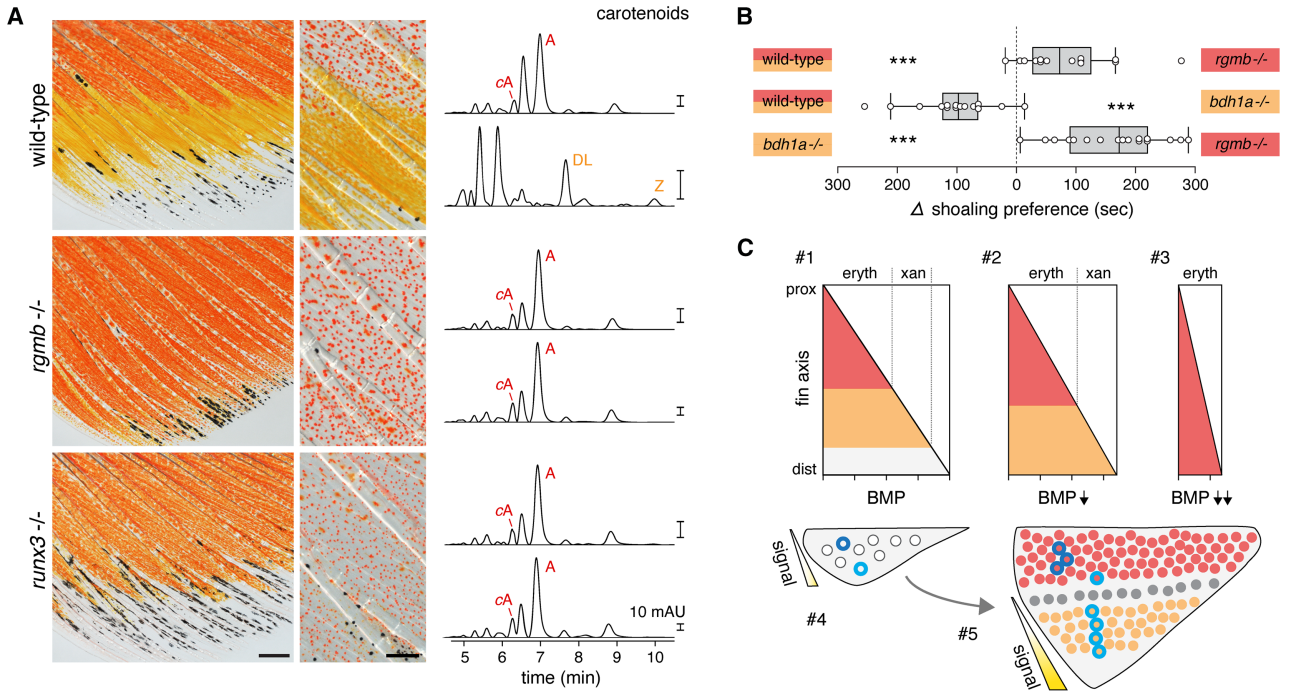

Figure 4. Variation in pigmentary phenotype and impacts on conspecific signal response in *D. albolineatus*

(A) *rgmb* and *runx3* mutants were deficient for yellow/orange xanthophores. Low- and high-magnification images were taken before and after epinephrine treatment, respectively. HPLC chromatographs (450 nm) are shown for proximal (upper) and distal (lower) fin regions from pooled fish in representative samples of each genotype. *c*A, *cis*-astanxanthin; A, astanxanthin; DL, dehydro-lutein; Z, zeaxanthin (see Data S1H).

(B) In assays of female shoaling, *rgmb*−/− males were preferred over wild type, and both wild-type and *rgmb*−/− males were preferred over red-deficient *bdh1a*−/− males. Points show differences in total times spent by individual females in proximity to each stimulus shoal (hypothesized mean difference = 0, Wilcoxon, $|S| \geq 49.5$, ***, $p < 0.001$; n = 14–17 fish tested). Boxes show medians with IQR, and bars are 1.5× IQR, with values for individual fish.

(C) Model for pigmentary phenotype dependence on BMP signaling and fin outgrowth. Alternative erythrophore and xanthophore fates from a common progenitor[15] depend on different upper and lower thresholds of BMP activity (#1). Genetic mosaic or pharmacological inhibitions of signaling (*gdf6a*, LDN-193189; #2) or more severe reductions due to biallelic mutations (*rgmb*−/−, *runx3*−/−; #3) alter fate specification and proximal-distal pattern boundaries. These effects occur in the context of extensive proximodistal outgrowth from ~0.5 mm base-to-tip when unspecified progenitors are first evident (#4) to ~2.2 mm when the earliest erythrophores and xanthophores are recognizable (#5). Prior fate mapping[15] showed that proximal progenitors (deep blue outline) produce erythrophores, whereas middle or distal progenitors (light blue outline) produce erythrophores and xanthophores or just xanthophores across the fin, with some progeny being displaced distally as the fin grows. Naturally occurring genetic variation exists for this phenotype, associated with chromosomal regions harboring genes of BMP and other pathways (Figure S7).

Scale bars, 500 (left) and 200 μm (right).

See also Figures S5–S10 and Data S1H and S1I.

xantholeucophores and xanthophore-like cells were deficient for yellow coloration, and defects in pattern orientation were evident; alterations in body and dorsal fin pigmentation were apparent as well (Figure S4D). These findings point to conserved roles for BMP signals in specifying patterns across taxa and chromatophore classes.

Phenotypes of zebrafish *rgmb* mutants and the presence of *rgmb* transcript in erythrophores and xanthophores (Figure S1E) led us to ask if the relative abundances of these cells might depend on Rgmb. Upon generating homozygous mutants for *rgmb* of *D. albolineatus* (Figure S5A), we found a marked increase in erythrophores, which extended to the distal tip of the fin, and a corresponding reduction in xanthophores (Figure 4A, left panels). Ectopic erythrophores of the mutant had densities more similar to wild-type proximal erythrophores than to distal xanthophores (Figure 4A, middle panels). Ectopic erythrophores also had large carotenoid vesicles, indistinguishable from wild-type erythrophores and larger than wild-type xanthophores (Figure S5B). Though BMP-inhibitor-treated *D. albolineatus* lacked clear defects in body pattern, a residual pattern of melanophore stripes, dorsal and ventral to an evolutionarily reduced interstripe,[43] was less organized and ultimately more diffuse in *rgmb*−/− than in the wild type (Figure S5C and see below).

Transcription factor Runx3[44] functions in concert with BMP signaling and downstream of Rgmb in zebrafish pigment cells.[36] Here, we found that *runx3* was expressed similarly to *rgmb* in erythrophores, xanthophores, and their progenitors (Figure S1H). To test if Runx3 functions likewise in *D. albolineatus*, we generated fish homozygous for premature termination alleles: these had phenotypes similar to *rgmb*−/−, albeit somewhat less severe (Figure 4A). This outcome—with those of pharmacological BMP inhibition and *gdf6a* mosaics—suggests roles for canonical and non-canonical BMP receptors, as well as conservation of a BMP/Runx3 module that affects pigment cell differentiation in *D. albolineatus*.

Please cite this article in press as: Huang et al., Graded BMP signals modulate yellow and red color in fishes, impacting adult pigment patterns and conspecific shoaling behavior, Current Biology (2026), https://doi.org/10.1016/j.cub.2026.03.007

Erythrophores and xanthophores contain different carotenoids, with red colors attributable to ketocarotenoids that are produced via enzymatic addition of ketone groups to yellow carotenoids.[11,15] The overtly red appearances of *rgmb* and *runx3* mutant *D. albolineatus* implied changes in carotenoid content, which we confirmed by high-performance liquid chromatography (Figure 4A, right panels). Examination of wild-type fish revealed multiple carotenoids in proximal fin regions, with a major peak corresponding to the ketocarotenoid astaxanthin, and distinct profiles of carotenoids in distal regions, including dehydro-lutein and zeaxanthin, which confer a yellow color (Figures S6A–S6C). *rgmb* and *runx3* mutants had significantly more astaxanthin than the wild type, and neither mutant had detectable dehydro-lutein or zeaxanthin. Conversely, fish with mutations in *bdh1a*, required for the formation of ketocarotenoids, lacked astaxanthin and had excess dehydro-lutein and zeaxanthin (Figures S6C and S6D; Data S1H).

Having identified a pathway and specific genes in this pathway required for the fin pigmentary phenotype, we were curious about the broader genetic architecture of this trait and whether there might be allelic variation available for selection. In some prior studies, we used a variant of the pearl danio, *D.* aff. *albolineatus*,[6,20] in which individuals often have erythrophores further distally and a redder appearance overall. We crossed *D.* aff. *albolineatus* and *D. albolineatus* and then crossed two F1s to generate a family of ~300 fish that had a wide range of phenotypes, from which we selected extreme yellow and extreme orange-red males that resembled *D. albolineatus* and *D.* aff. *albolineatus*, respectively (Figures S7A and S7B). Whole-genome sequencing and mapping revealed weak associations with phenotype across several chromosomes and a highly significant association that spanned Chr23, harboring about two dozen plausible candidate genes (Figures S7C and S8–S10; Data S1I). These findings indicated standing genetic variation and hint at an oligogenic basis for populational variability in pigmentary traits, as for other *Danio*.[45]

Finally, with a deeper understanding of developmental mechanisms and variation, we asked if these phenotypes impact behavior, as might be anticipated given roles for red, orange, or yellow colors as signals in mate choice, social aggregation, and dominance displays.[46–50] We focused on a social aggregative behavior, shoaling, important for predation avoidance, foraging efficiency, and access to mates.[51] Zebrafish associate based on pigmentary and other factors[52–54] but cues used by *D. albolineatus* in shoaling with conspecifics are not known. We reasoned that isolation of extreme phenotypes beyond those of wild type ("super-red" *rgmb* and red-deficient *bdh1a*; Figures S10A and S10B) provided an opportunity to test if these colors impact shoaling.

Proximity to conspecifics is a necessary prelude to mate choice, and *D. albolineatus* is sexually dimorphic, with males redder than females,[15] so we tested shoaling of females in binary preference assays using alternative male phenotypes. When presented with wild-type and *rgmb* mutants, females preferred *rgmb*−/− (Figures 4B and S10C). This preference could indicate that *rgmb* mutants provide a sign stimulus exceeding wild type or that females are attracted to novelty, independent of specific color.[8,55] Consistent with the former possibility, females preferred wild type over red-deficient *bdh1a*−/− and even more strongly preferred *rgmb*−/− over *bdh1a*−/−.

Taken together, these analyses support a model in which redder coloration—imparted by carotenoids and preferred by females when choosing shoal mates—depends on BMP signaling and segregating variants that may include genes of this and other pathways. During ontogeny (Figure 4C), progenitor cells experience different levels of BMP signaling that promote specification and differentiation as erythrophores (low levels) or xanthophores (intermediate to high) or that permit neither fate (highest). Because ligand gene expression is biased distally in the outgrowing fin and developing chromatophores are equipped with several BMP receptors (including Rgmb), thresholds for fate lead to proximal-distal patterns. If signals are attenuated, locally produced fates are altered, and pattern features are displaced. Importantly, these events unfold in the context of growth and changes in positions[16]: some chromatophores are carried distally as the region of highest signaling grows distally, and other chromatophores remain proximally as the fin tip grows away from them. These dynamics make it likely that developing chromatophores interpret thresholds for specification by integrating both signal amplitude and duration. Nevertheless, we cannot exclude the possibility of cell-type-specific activities of ligands or receptors that would uniquely specify one fate over another nor can we rule out the possibility that females might prefer some other attribute of *rgmb*−/− over wild type.

The developmental genetic dissection we have undertaken provides insights into the origins of a trait that can serve as a behavioral signal to conspecifics. Our demonstration that the pathway functions in multiple species to influence pattern further suggests a generalized mechanism. With this backdrop, one can envisage how historical contingencies across phylogenetic lineages have led to species-specific patterns, reflecting complements of available chromatophores, variation that has arisen for signal availability and chromatophore-lineage responsiveness, and the broader behavioral and ecological context of selection. Beyond fins and pigmentation, contributions of BMP signaling are evident for beetle horns and have been suggested for the combs of chickens,[56] antlers of deer,[57] and other exaggerated structures relevant to animal communication and often occurring at anatomical extremities.[58] The pathway might be especially co-optable for such roles, given functions in appendage outgrowth[52–54,59] and skin appendage patterning (feathers, hair, and scales)[60] and the potential for evolutionary fine-tuning of gradients, cell-type-specific thresholds, and allometric relationships.

RESOURCE AVAILABILITY

Lead contact

Requests for further information and resources should be directed to and will be fulfilled by the lead contact, David M. Parichy (dparichy@virginia.edu).

Materials availability

All unique/stable reagents generated in this study are available from the lead contact without restriction.

Data and code availability

- Transcriptomic and genomic sequencing data are available at NCBI SRA/BioProject identifier PRJNA1365945.
- This paper does not report original code.
- Any additional information required to reanalyze the data reported in this paper is available from the lead contact upon request.

ACKNOWLEDGMENTS

This work was supported by NIH R35 GM122471 to D.M.P. We thank the Parichy lab members for assistance with fish care, T.A. Larson and L.B. Patterson for helpful discussions and advice, and Sarah Wilmsen and the University of Virginia Journal of Molecular Electron Microscopy core for assistance with electron microscopy.

AUTHOR CONTRIBUTIONS

D.M.P. and D.H. conceptualized the experiments. D.H., T.L., E.H.K., Y. Liang, and Y. Liu conducted the experiments, supervised by D.M.P. and J.C.C. J.L. contributed unpublished genomic annotations. D.M.P., D.H., P.L.H.d.M., Y. Liu, and J.C.C. analyzed the data. D.M.P. and D.H. wrote the manuscript.

DECLARATION OF INTERESTS

The authors declare no competing interests.

STAR★METHODS

Detailed methods are provided in the online version of this paper and include the following:

- KEY RESOURCES TABLE
- EXPERIMENTAL MODEL AND STUDY PARTICIPANT DETAILS
- METHOD DETAILS
  - CRISPR/Cas9 Mutagenesis
  - Pharmacological Analysis
  - Carotenoid Analyses
  - Immunohistochemical Staining
  - Lineage Tracing
  - Imaging and Image Processing
  - Transmission Electron Microscopy (TEM)
  - Bulk RNA-Seq and Single-cell RNA-Seq
  - Genome Assembly and Annotation
  - Bulk Segregant Analysis
- SHOALING PREFERENCE ASSAY
- QUANTIFICATION AND STATISTICAL ANALYSES

SUPPLEMENTAL INFORMATION

Supplemental information can be found online at https://doi.org/10.1016/j.cub.2026.03.007.

Received: December 5, 2025
Revised: February 3, 2026
Accepted: March 3, 2026

REFERENCES

1. Cuthill, I.C., Allen, W.L., Arbuckle, K., Caspers, B., Chaplin, G., Hauber, M.E., Hill, G.E., Jablonski, N.G., Jiggins, C.D., Kelber, A., et al. (2017). The biology of color. Science *357*, eaan0221. https://doi.org/10.1126/science.aan0221.
2. Endler, J.A., and Mappes, J. (2017). The current and future state of animal coloration research. Philos. Trans. R. Soc. Lond. B Biol. Sci. *372*, 20160352. https://doi.org/10.1098/rstb.2016.0352.
3. Svensson, P.A., and Wong, B.B.M. (2011). Carotenoid-based signals in behavioural ecology: a review. Behaviour *148*, 131–189. https://doi.org/10.1163/000579510x548673.
4. Parichy, D.M. (2021). Evolution of pigment cells and patterns: recent insights from teleost fishes. Curr. Opin. Genet. Dev. *69*, 88–96. https://doi.org/10.1016/j.gde.2021.02.006.
5. Kratochwil, C.F., and Mallarino, R. (2023). Mechanisms Underlying the Formation and Evolution of Vertebrate Color Patterns. Annu. Rev. Genet. *57*, 135–156. https://doi.org/10.1146/annurev-genet-031423-120918.
6. Parichy, D.M. (2015). Advancing biology through a deeper understanding of zebrafish ecology and evolution. eLife *4*, e05635. https://doi.org/10.7554/eLife.05635.
7. Irschick, D.J., Briffa, M., and Podos, J. (2015). Animal Signaling and Function: an Integrative Approach (John Wiley & Sons, Inc.). https://doi.org/10.1002/9781118966624.
8. Tinbergen, N. (1951). The Study of Instinct (Oxford University Press).
9. Weaver, R.J., Koch, R.E., and Hill, G.E. (2017). What maintains signal honesty in animal colour displays used in mate choice? Philos. Trans. R. Soc. Lond. B Biol. Sci. *372*, 20160343. https://doi.org/10.1098/rstb.2016.0343.
10. Hill, G.E., Weaver, R.J., and Powers, M.J. (2023). Carotenoid ornaments and the spandrels of physiology: a critique of theory to explain condition dependency. Biol. Rev. Camb. Philos. Soc. *98*, 2320–2332. https://doi.org/10.1111/brv.13008.
11. Toomey, M.B., Marques, C.I., Araújo, P.M., Huang, D., Zhong, S., Liu, Y., Schreiner, G.D., Myers, C.A., Pereira, P., Afonso, S., et al. (2022). A mechanism for red coloration in vertebrates. Curr. Biol. *32*, 4201–4214.e12. https://doi.org/10.1016/j.cub.2022.08.013.
12. Schartl, M., Larue, L., Goda, M., Bosenberg, M.W., Hashimoto, H., and Kelsh, R.N. (2016). What is a vertebrate pigment cell? Pigment Cell Melanoma Res. *29*, 8–14. https://doi.org/10.1111/pcmr.12409.
13. McCluskey, B.M., and Postlethwait, J.H. (2015). Phylogeny of zebrafish, a "model species," within Danio, a "model genus". Mol. Biol. Evol. *32*, 635–652. https://doi.org/10.1093/molbev/msu325.
14. Lu, J., Podobnik, M., Huang, J., McCluskey, B.M., McCarthy, S.A., Wood, J., Collins, J., Torrance, J., Sims, Y., Gao, D., et al. (2025). Genomic and genetic insights into speciation and pigment pattern diversification in Danio fishes. bioRxiv, 2025.10.17.682988. https://doi.org/10.1101/2025.10.17.682988.
15. Huang, D., Lewis, V.M., Foster, T.N., Toomey, M.B., Corbo, J.C., and Parichy, D.M. (2021). Development and genetics of red coloration in the zebrafish relative Danio albolineatus. eLife *10*, e70253. https://doi.org/10.7554/eLife.70253.
16. Goodrich, H.B., and Greene, J.M. (1959). An experimental analysis of the development of a color pattern in the fish Brachydanio albolineatus Blyth. J. Exp. Zool. *141*, 15–45. https://doi.org/10.1002/jez.1401410103.
17. Granneman, J.G., Kimler, V.A., Zhang, H., Ye, X., Luo, X., Postlethwait, J.H., and Thummel, R. (2017). Lipid droplet biology and evolution illuminated by the characterization of a novel perilipin in teleost fish. eLife *6*, e21771. https://doi.org/10.7554/eLife.21771.
18. Toomey, M.B., Lopes, R.J., Araújo, P.M., Johnson, J.D., Gazda, M.A., Afonso, S., Mota, P.G., Koch, R.E., Hill, G.E., Corbo, J.C., et al. (2017). High-density lipoprotein receptor SCARB1 is required for carotenoid coloration in birds. Proc. Natl. Acad. Sci. USA *114*, 5219–5224. https://doi.org/10.1073/pnas.1700751114.
19. Tu, S., and Johnson, S.L. (2010). Clonal analyses reveal roles of organ founding stem cells, melanocyte stem cells and melanoblasts in establishment, growth and regeneration of the adult zebrafish fin. Development *137*, 3931–3939. https://doi.org/10.1242/dev.057075.
20. Quigley, I.K., Manuel, J.L., Roberts, R.A., Nuckels, R.J., Herrington, E.R., MacDonald, E.L., and Parichy, D.M. (2005). Evolutionary diversification of pigment pattern in Danio fishes: differential fms dependence and stripe loss in D. albolineatus. Development *132*, 89–104. https://doi.org/10.1242/dev.01547.
21. Patterson, L.B., Bain, E.J., and Parichy, D.M. (2014). Pigment cell interactions and differential xanthophore recruitment underlying zebrafish stripe reiteration and Danio pattern evolution. Nat. Commun. *5*, 5299. https://doi.org/10.1038/ncomms6299.
22. Bier, E., and De Robertis, E.M. (2015). EMBRYO DEVELOPMENT. BMP gradients: A paradigm for morphogen-mediated developmental patterning. Science *348*, aaa5838. https://doi.org/10.1126/science.aaa5838.

23. Mosby, L.S., Bowen, A.E., and Hadjivasiliou, Z. (2024). Morphogens in the evolution of size, shape and patterning. Development *151*, dev202412. https://doi.org/10.1242/dev.202412.

24. Raspopovic, J., Marcon, L., Russo, L., and Sharpe, J. (2014). Modeling digits. Digit patterning is controlled by a Bmp-Sox9-Wnt Turing network modulated by morphogen gradients. Science *345*, 566–570. https://doi.org/10.1126/science.1252960.

25. Hill, C.S. (2022). Establishment and interpretation of NODAL and BMP signaling gradients in early vertebrate development. Curr. Top. Dev. Biol. *149*, 311–340. https://doi.org/10.1016/bs.ctdb.2021.12.002.

26. Camacho-Aguilar, E., Yoon, S.T., Ortiz-Salazar, M.A., Du, S., Guerra, M.C., and Warmflash, A. (2024). Combinatorial interpretation of BMP and WNT controls the decision between primitive streak and extraembryonic fates. Cell Syst. *15*, 445–461.e4. https://doi.org/10.1016/j.cels.2024.04.001.

27. Andrews, M.G., Del Castillo, L.M., Ochoa-Bolton, E., Yamauchi, K., Smogorzewski, J., and Butler, S.J. (2017). BMPs direct sensory interneuron identity in the developing spinal cord using signal-specific not morphogenic activities. eLife *6*, e30647. https://doi.org/10.7554/eLife.30647.

28. Duval, N., Vaslin, C., Barata, T.C., Frarma, Y., Contremoulins, V., Baudin, X., Nedelec, S., and Ribes, V.C. (2019). BMP4 patterns Smad activity and generates stereotyped cell fate organization in spinal organoids. Development *146*, dev175430. https://doi.org/10.1242/dev.175430.

29. Mateus, R., Holtzer, L., Seum, C., Hadjivasiliou, Z., Dubois, M., Jülicher, F., and Gonzalez-Gaitan, M. (2020). BMP Signaling Gradient Scaling in the Zebrafish Pectoral Fin. Cell Rep. *30*, 4292–4302.e7. https://doi.org/10.1016/j.celrep.2020.03.024.

30. Thorimbert, V., König, D., Marro, J., Ruggiero, F., and Jaźwińska, A. (2015). Bone morphogenetic protein signaling promotes morphogenesis of blood vessels, wound epidermis, and actinotrichia during fin regeneration in zebrafish. FASEB J. *29*, 4299–4312. https://doi.org/10.1096/fj.15-272955.

31. Klammert, U., Mueller, T.D., Hellmann, T.V., Wuerzler, K.K., Kotzsch, A., Schliermann, A., Schmitz, W., Kuebler, A.C., Sebald, W., and Nickel, J. (2015). GDF-5 can act as a context-dependent BMP-2 antagonist. BMC Biol. *13*, 77. https://doi.org/10.1186/s12915-015-0183-8.

32. Kodama, N., Matsubara, T., Yoshimura, A., Nagano, K., Hino, J., Tsuji, K., Ikedo, A., Imai, Y., Yaginuma, T., Yuan, Q., et al. (2025). BMP3b regulates bone mass by inhibiting BMP signaling. Bone *190*, 117303. https://doi.org/10.1016/j.bone.2024.117303.

33. Gramann, A.K., Venkatesan, A.M., Guerin, M., and Ceol, C.J. (2019). Regulation of zebrafish melanocyte development by ligand-dependent BMP signaling. eLife *8*, e50047. https://doi.org/10.7554/eLife.50047.

34. Venkatesan, A.M., Vyas, R., Gramann, A.K., Dresser, K., Gujja, S., Bhatnagar, S., Chhangawala, S., Gomes, C.B.F., Xi, H.S., Lian, C.G., et al. (2018). Ligand-activated BMP signaling inhibits cell differentiation and death to promote melanoma. J. Clin. Investig. *128*, 294–308. https://doi.org/10.1172/JCI92513.

35. Yu, P.B., Deng, D.Y., Lai, C.S., Hong, C.C., Cuny, G.D., Bouxsein, M.L., Hong, D.W., McManus, P.M., Katagiri, T., Sachidanandan, C., et al. (2008). BMP type I receptor inhibition reduces heterotopic [corrected] ossification. Nat. Med. *14*, 1363–1369. https://doi.org/10.1038/nm.1888.

36. Huang, D., Kapadia, E.H., Liang, Y., Shriver, L.P., Dai, S., Patti, G.J., Humbel, B.M., Laudet, V., and Parichy, D.M. (2025). Agouti and BMP signaling drive a naturally occurring fate conversion of melanophores to leucophores in zebrafish. Proc. Natl. Acad. Sci. USA *122*, e2424180122. https://doi.org/10.1073/pnas.2424180122.

37. Mills, M.G., Nuckels, R.J., and Parichy, D.M. (2007). Deconstructing evolution of adult phenotypes: genetic analyses of kit reveal homology and evolutionary novelty during adult pigment pattern development of Danio fishes. Development *134*, 1081–1090. https://doi.org/10.1242/dev.02799.

38. Tang, K.L., Agnew, M.K., Hirt, M.V., Sado, T., Schneider, L.M., Freyhof, J., Sulaiman, Z., Swartz, E., Vidthayanon, C., Miya, M., et al. (2010). Systematics of the subfamily Danioninae (Teleostei: Cypriniformes: Cyprinidae). Mol. Phylogenet. Evol. *57*, 189–214. https://doi.org/10.1016/j.ympev.2010.05.021.

39. Gur, D., Bain, E.J., Johnson, K.R., Aman, A.J., Pasolli, H.A., Flynn, J.D., Allen, M.C., Deheyn, D.D., Lee, J.C., Lippincott-Schwartz, J., et al. (2020). In situ differentiation of iridophore crystallotypes underlies zebrafish stripe patterning. Nat. Commun. *11*, 6391. https://doi.org/10.1038/s41467-020-20088-1.

40. Lewis, V.M., Saunders, L.M., Larson, T.A., Bain, E.J., Sturiale, S.L., Gur, D., Chowdhury, S., Flynn, J.D., Allen, M.C., Deheyn, D.D., et al. (2019). Fate plasticity and reprogramming in genetically distinct populations of Danio leucophores. Proc. Natl. Acad. Sci. USA *116*, 11806–11811. https://doi.org/10.1073/pnas.1901021116.

41. Huang, D., Liu, T., Carr, A.A., de Mello, P.H., Liang, Y., Shriver, L.P., Chauvigné, F., Johnson, S.L., Cerdà, J., Patti, G.J., et al. (2026). Cell type diversification and phenotype convergence underlying white fin-ornamentation of cyprinid fishes. Proc. Natl. Acad. Sci. USA *123*, e2537571123. https://doi.org/10.1073/pnas/2537571123.

42. Zhang, J., Jiang, Y., Zhang, Z., Li, S., Fan, H., Gu, J., Mao, R., and Xu, X. (2024). Repulsive guidance molecules b (RGMb): molecular mechanism, function and role in diseases. Expert Rev. Mol. Med. *26*, e24. https://doi.org/10.1017/erm.2024.24.

43. McCluskey, B.M., Liang, Y., Lewis, V.M., Patterson, L.B., and Parichy, D.M. (2021). Pigment pattern morphospace of Danio fishes: evolutionary diversification and mutational effects. Biol. Open *10*, bio058814. https://doi.org/10.1242/bio.058814.

44. Mevel, R., Draper, J.E., Lie-A-Ling, M., Kouskoff, V., and Lacaud, G. (2019). RUNX transcription factors: orchestrators of development. Development *146*, dev148296. https://doi.org/10.1242/dev.148296.

45. McCluskey, B.M., Uji, S., Mancusi, J.L., Postlethwait, J.H., and Parichy, D.M. (2021). A complex genetic architecture in zebrafish relatives Danio quagga and D. kyathit underlies development of stripes and spots. PLoS Genet. *17*, e1009364. https://doi.org/10.1371/journal.pgen.1009364.

46. Toomey, M.B., and McGraw, K.J. (2012). Mate choice for a male carotenoid-based ornament is linked to female dietary carotenoid intake and accumulation. BMC Evol. Biol. *12*, 3. https://doi.org/10.1186/1471-2148-12-3.

47. Grether, G.F., Hudon, J., and Endler, J.A. (2001). Carotenoid scarcity, synthetic pteridine pigments and the evolution of sexual coloration in guppies (Poecilia reticulata). Proc. Biol. Sci. *268*, 1245–1253. https://doi.org/10.1098/rspb.2001.1624.

48. Kim, S.Y., and Velando, A. (2014). Stickleback Males Increase Red Coloration and Courtship Behaviours in the Presence of a Competitive Rival. Ethology *120*, 502–510. https://doi.org/10.1111/eth.12224.

49. Takahashi, D. (2018). Female Mate Choice Based on Male Nuptial Coloration in Pale Chub, Zacco platypus. Zool. Sci. *35*, 23–27. https://doi.org/10.2108/zs170102.

50. Milinski, M., and Bakker, T.C.M. (1990). Female Sticklebacks Use Male Coloration in Mate Choice and Hence Avoid Parasitized Males. Nature *344*, 330–333. https://doi.org/10.1038/344330a0.

51. Ward, A.J.W., Kent, M.I.A., and Webster, M.M. (2020). Social Recognition and Social Attraction in Group-Living Fishes. Front. Ecol. Evol. *8*, 15. https://doi.org/10.3389/fevo.2020.00015.

52. Engeszer, R.E., Wang, G., Ryan, M.J., and Parichy, D.M. (2008). Sex-specific perceptual spaces for a vertebrate basal social aggregative behavior. Proc. Natl. Acad. Sci. USA *105*, 929–933. https://doi.org/10.1073/pnas.0708778105.

53. Engeszer, R.E., Barbiano, L.A.D., Ryan, M.J., and Parichy, D.M. (2007). Timing and plasticity of shoaling behaviour in the zebrafish, Danio rerio. Anim. Behav. *74*, 1269–1275. https://doi.org/10.1016/j.anbehav.2007.01.032.

54. Spence, R., and Smith, C. (2007). The role of early learning in determining shoaling preferences based on visual cues in the zebrafish, Danio rerio. Ethology *113*, 62–67. https://doi.org/10.1111/J.1439-0310.2006.01295.X.

55. Potter, T., Arendt, J., Bassar, R.D., Watson, B., Bentzen, P., Travis, J., and Reznick, D.N. (2023). Female preference for rare males is maintained by indirect selection in Trinidadian guppies. Science *380*, 309–312. https://doi.org/10.1126/science.ade5671.

56. Johnsson, M., Gustafson, I., Rubin, C.J., Sahlqvist, A.S., Jonsson, K.B., Kerje, S., Ekwall, O., Kämpe, O., Andersson, L., Jensen, P., et al. (2012). A sexual ornament in chickens is affected by pleiotropic alleles at HAO1 and BMP2, selected during domestication. PLoS Genet. *8*, e1002914. https://doi.org/10.1371/journal.pgen.1002914.

57. Pita-Thomas, W., Fernández-Martos, C., Yunta, M., Maza, R.M., Navarro-Ruiz, R., Lopez-Rodríguez, M.J., Reigada, D., Nieto-Sampedro, M., and Nieto-Diaz, M. (2010). Gene expression of axon growth promoting factors in the deer antler. PLoS One *5*, e15706. https://doi.org/10.1371/journal.pone.0015706.

58. Kang, J.H. (2024). The Genetic Basis Underpinning Sexually Selected Traits across Different Animal Lineages: Are There Genetic Mechanisms in Common? Animals (Basel) *14*, 841. https://doi.org/10.3390/ani14060841.

59. Barrio, L., and Milán, M. (2017). Boundary Dpp promotes growth of medial and lateral regions of the Drosophila wing. eLife *6*, e22013. https://doi.org/10.7554/eLife.22013.

60. Chang, W.L., Wu, H., Chiu, Y.K., Wang, S., Jiang, T.X., Luo, Z.L., Lin, Y.C., Li, A., Hsu, J.T., Huang, H.L., et al. (2019). The Making of a Flight Feather: Bio-architectural Principles and Adaptation. Cell *179*, 1409–1423.e17. https://doi.org/10.1016/j.cell.2019.11.008.

61. Parichy, D.M., Rawls, J.F., Pratt, S.J., Whitfield, T.T., and Johnson, S.L. (1999). Zebrafish sparse corresponds to an orthologue of c-kit and is required for the morphogenesis of a subpopulation of melanocytes, but is not essential for hematopoiesis or primordial germ cell development. Development *126*, 3425–3436. https://doi.org/10.1242/dev.126.15.3425.

62. Bray, N.L., Pimentel, H., Melsted, P., and Pachter, L. (2016). Near-optimal probabilistic RNA-seq quantification. Nat. Biotechnol. *34*, 525–527. https://doi.org/10.1038/nbt.3519.

63. Love, M.I., Huber, W., and Anders, S. (2014). Moderated estimation of fold change and dispersion for RNA-seq data with DESeq2. Genome Biol. *15*, 550. https://doi.org/10.1186/s13059-014-0550-8.

64. Trapnell, C., Cacchiarelli, D., Grimsby, J., Pokharel, P., Li, S., Morse, M., Lennon, N.J., Livak, K.J., Mikkelsen, T.S., and Rinn, J.L. (2014). The dynamics and regulators of cell fate decisions are revealed by pseudotemporal ordering of single cells. Nat. Biotechnol. *32*, 381–386. https://doi.org/10.1038/nbt.2859.

65. Cao, J., Spielmann, M., Qiu, X., Huang, X., Ibrahim, D.M., Hill, A.J., Zhang, F., Mundlos, S., Christiansen, L., Steemers, F.J., et al. (2019). The single-cell transcriptional landscape of mammalian organogenesis. Nature *566*, 496–502. https://doi.org/10.1038/s41586-019-0969-x.

66. Brown, D., and Cox, A.J. (2009). Innovative Uses of Video Analysis. Phys. Teach. *47*, 145–150. https://doi.org/10.1119/1.3081296.

67. Parichy, D.M., Elizondo, M.R., Mills, M.G., Gordon, T.N., and Engeszer, R.E. (2009). Normal table of postembryonic zebrafish development: staging by externally visible anatomy of the living fish. Dev. Dyn. *238*, 2975–3015. https://doi.org/10.1002/dvdy.22113.

68. Hoshijima, K., Jurynec, M.J., Klatt Shaw, D., Jacobi, A.M., Behlke, M.A., and Grunwald, D.J. (2019). Highly Efficient CRISPR-Cas9-Based Methods for Generating Deletion Mutations and F0 Embryos that Lack Gene Function in Zebrafish. Dev. Cell *51*, 645–657.e4. https://doi.org/10.1016/j.devcel.2019.10.004.

69. Elizarraras, J.M., Liao, Y., Shi, Z., Zhu, Q., Pico, A.R., and Zhang, B. (2024). WebGestalt 2024: faster gene set analysis and new support for metabolomics and multi-omics. Nucleic Acids Res. *52*, W415–W421. https://doi.org/10.1093/nar/gkae456.

70. Baxter, L.L., Watkins-Chow, D.E., Pavan, W.J., and Loftus, S.K. (2019). A curated gene list for expanding the horizons of pigmentation biology. Pigment Cell Melanoma Res. *32*, 348–358. https://doi.org/10.1111/pcmr.12743.

71. Barnett, D.W., Garrison, E.K., Quinlan, A.R., Strömberg, M.P., and Marth, G.T. (2011). BamTools: a C++ API and toolkit for analyzing and managing BAM files. Bioinformatics *27*, 1691–1692. https://doi.org/10.1093/bioinformatics/btr174.

72. De Coster, W., and Rademakers, R. (2023). NanoPack2: population-scale evaluation of long-read sequencing data. Bioinformatics *39*, btad311. https://doi.org/10.1093/bioinformatics/btad311.

73. Cheng, H., Concepcion, G.T., Feng, X., Zhang, H., and Li, H. (2021). Haplotype-resolved de novo assembly using phased assembly graphs with hifiasm. Nat. Methods *18*, 170–175. https://doi.org/10.1038/s41592-020-01056-5.

74. Gurevich, A., Saveliev, V., Vyahhi, N., and Tesler, G. (2013). QUAST: quality assessment tool for genome assemblies. Bioinformatics *29*, 1072–1075. https://doi.org/10.1093/bioinformatics/btt086.

75. Manni, M., Berkeley, M.R., Seppey, M., Simão, F.A., and Zdobnov, E.M. (2021). BUSCO Update: Novel and Streamlined Workflows along with Broader and Deeper Phylogenetic Coverage for Scoring of Eukaryotic, Prokaryotic, and Viral Genomes. Mol. Biol. Evol. *38*, 4647–4654. https://doi.org/10.1093/molbev/msab199.

76. Alonge, M., Lebeigle, L., Kirsche, M., Jenike, K., Ou, S., Aganezov, S., Wang, X., Lippman, Z.B., Schatz, M.C., and Soyk, S. (2022). Automated assembly scaffolding using RagTag elevates a new tomato system for high-throughput genome editing. Genome Biol. *23*, 258. https://doi.org/10.1186/s13059-022-02823-7.

77. Howe, K., Clark, M.D., Torroja, C.F., Torrance, J., Berthelot, C., Muffato, M., Collins, J.E., Humphray, S., McLaren, K., Matthews, L., et al. (2013). The zebrafish reference genome sequence and its relationship to the human genome. Nature *496*, 498–503. https://doi.org/10.1038/nature12111.

78. Flynn, J.M., Hubley, R., Goubert, C., Rosen, J., Clark, A.G., Feschotte, C., and Smit, A.F. (2020). RepeatModeler2 for automated genomic discovery of transposable element families. Proc. Natl. Acad. Sci. USA *117*, 9451–9457. https://doi.org/10.1073/pnas.1921046117.

79. Smit, A.F.A., Hubley, R., and Green, P. (2013–2015), RepeatMasker Open-4.0. http://www.repeatmasker.org

80. Bao, W., Kojima, K.K., and Kohany, O. (2015). Repbase Update, a database of repetitive elements in eukaryotic genomes. Mobile DNA *6*, 11. https://doi.org/10.1186/s13100-015-0041-9.

81. Quinlan, A.R., and Hall, I.M. (2010). BEDTools: a flexible suite of utilities for comparing genomic features. Bioinformatics *26*, 841–842. https://doi.org/10.1093/bioinformatics/btq033.

82. Shumate, A., and Salzberg, S.L. (2021). Liftoff: accurate mapping of gene annotations. Bioinformatics *37*, 1639–1643. https://doi.org/10.1093/bioinformatics/btaa1016.

83. Chen, S., Zhou, Y., Chen, Y., and Gu, J. (2018). fastp: an ultra-fast all-in-one FASTQ preprocessor. Bioinformatics *34*, i884–i890. https://doi.org/10.1093/bioinformatics/bty560.

84. Langmead, B., and Salzberg, S.L. (2012). Fast gapped-read alignment with Bowtie 2. Nat. Methods *9*, 357–359. https://doi.org/10.1038/nmeth.1923.

85. Danecek, P., Bonfield, J.K., Liddle, J., Marshall, J., Ohan, V., Pollard, M.O., Whitwham, A., Keane, T., McCarthy, S.A., Davies, R.M., et al. (2021). Twelve years of SAMtools and BCFtools. GigaScience *10*, giab008. https://doi.org/10.1093/gigascience/giab008.

86. Kofler, R., Pandey, R.V., and Schlötterer, C. (2011). PoPoolation2: identifying differentiation between populations using sequencing of pooled DNA samples (Pool-Seq). Bioinformatics *27*, 3435–3436. https://doi.org/10.1093/bioinformatics/btr589.

87. Mansfeld, B.N., and Grumet, R. (2018). QTLseqr: An R Package for Bulk Segregant Analysis with Next-Generation Sequencing. Plant Genome *11*. https://doi.org/10.3835/plantgenome2018.01.0006.

88. Magwene, P.M., Willis, J.H., and Kelly, J.K. (2011). The statistics of bulk segregant analysis using next generation sequencing. PLoS Comput. Biol. *7*, e1002255. https://doi.org/10.1371/journal.pcbi.1002255.

89. Benjamini, Y., and Hochberg, Y. (1995). Controlling the False Discovery Rate: A Practical and Powerful Approach to Multiple Testing. J. R. Stat. Soc., B (Methodol.) *57*, 289–300. https://doi.org/10.1111/j.2517-6161.1995.tb02031.x.

90. Cingolani, P., Platts, A., Wang le, L., Coon, M., Nguyen, T., Wang, L., Land, S.J., Lu, X., and Ruden, D.M. (2012). A program for annotating and predicting the effects of single nucleotide polymorphisms, SnpEff: SNPs in the genome of Drosophila melanogaster strain w1118; iso-2; iso-3. Fly (Austin) *6*, 80–92. https://doi.org/10.4161/fly.19695.

91. Tajima, F. (1989). Statistical method for testing the neutral mutation hypothesis by DNA polymorphism. Genetics *123*, 585–595. https://doi.org/10.1093/genetics/123.3.585.

92. Czech, L., Spence, J.P., and Expósito-Alonso, M. (2024). grenedalf: population genetic statistics for the next generation of pool sequencing. Bioinformatics *40*, btae508. https://doi.org/10.1093/bioinformatics/btae508.

Please cite this article in press as: Huang et al., Graded BMP signals modulate yellow and red color in fishes, impacting adult pigment patterns and conspecific shoaling behavior, Current Biology (2026), https://doi.org/10.1016/j.cub.2026.03.007

STAR★METHODS

KEY RESOURCES TABLE

REAGENT or RESOURCE	SOURCE	IDENTIFIER
Antibodies		
Rabbit monoclonal anti- Phospho-Smad1 (Ser463/465)/ Smad5 (Ser463/465)/ Smad9 (Ser465/467)	Cell Signaling Technology	Cat# 13820; RRID:AB_2493181
Goat anti-rabbit Alexa Fluor Plus 647	Invitrogen	Cat# A32732; RRID:AB_2633281
DAPI	Invitrogen	Cat # D1306; RRID:AB_2629482
Chemicals, peptides, and recombinant proteins		
LDN-193189	Selleck Chemicals	Cat# S7507
DMSO	Fisher Scientific	Cat# D128-1
MS222	Millipore Sigma	Cat# A5040
Epinephrine Hydrochloride	Sigma-Aldrich	Cat# E4642
Liberase	Roche	Cat# 5401119001
Alt-R™ S.p. Cas9 Nuclease V3	IDT	Cat# 1081058
Critical commercial assays		
RNAqueous™-Micro Total RNA Isolation Kit	Thermo Fisher	Cat# AM1931
Chromium Next GEM Single Cell 3' Kit v3.1	10x Genomics	Cat# PN-1000268
SMART-Seq mRNA LP kit	Takara	Cat# 634768
NSQ 500/550 Hi Output KT v2.5 (150 CYS)	Illumina	Cat# 20024907
Deposited data		
RNA sequencing and genomic sequencing data	SRA	PRJNA1365945
Experimental models: Organisms/strains		
Danio albolineatus: *Tg(aox5:nucEos)*^{vp37albTg}	Huang et al.[15]	N/A
Danio albolineatus: kita-/-	Mills et al.[37] Parichy et al.[61]	N/A
Danio albolineatus: *rgmb*^{vp67al1}	This paper	N/A
Danio albolineatus: *rgmb*^{vp67al2}	This paper	N/A
Danio albolineatus: *bdh1a*^{vp40ac1}	Huang et al.[15]	N/A
Danio albolineatus: *runx3*^{vp68a1}	This paper	N/A
Danio albolineatus: *runx3*^{vp68a2}	This paper	N/A
Danio aff. *albolineatus*	Quigley et al.[20]	N/A
Zebrafish: *rgmb*^{vp67re1}	Huang et al.[36]	N/A
Tanichthys albonubes	The Wet Spot Tropical Fish	https://www.wetspottropicalfish.com/product/tanichthys-albonubes/
Oligonucleotides		
AltR gRNA targeting *gdf6a*: ATGTAGTCGTGAGGCACAAC	IDT	CD.Cas9.DLGD6978.AC
AltR gRNA targeting *rgmb*: AGAGGAACTGCTCCAAAGAC	IDT	CD.Cas9.BWRG6584.AB
AltR gRNA targeting *runx3*: ACCCTGGAAACGGGACCACC	IDT	CD.Cas9.SMRN1496.AA
Software and algorithms		
Kallisto	Bray et al.[62]	https://pachterlab.github.io/kallisto/
DESeq2	Love et al.[63]	https://github.com/thelovelab/DESeq2
Cell Ranger	10x Genomics	https://www.10xgenomics.com/support/software/cell-ranger/latest
Monocle3	Trapnell et al.[64] Cao et al.[65]	https://cole-trapnell-lab.github.io/monocle3/
JMP Pro 18	SAS Institute	https://www.jmp.com/

(*Continued on next page*)

Please cite this article in press as: Huang et al., Graded BMP signals modulate yellow and red color in fishes, impacting adult pigment patterns and conspecific shoaling behavior, Current Biology (2026), https://doi.org/10.1016/j.cub.2026.03.007

Continued

REAGENT or RESOURCE	SOURCE	IDENTIFIER
Tracker	Brown and Cox[66]	https://opensourcephysics.github.io/tracker-website/
ZEN blue	Zeiss	https://www.zeiss.com/microscopy/us/products/software/zeiss-zen.html
ZEN black	Zeiss	https://www.zeiss.com/microscopy/us/products/software/zeiss-zen.html

EXPERIMENTAL MODEL AND STUDY PARTICIPANT DETAILS

Danio albolineatus were derived from individuals collected in Thailand by M. McClure in 1995, subsequently provided to the laboratory of S. Johnson (dec.), and have been maintained as a closed stock in our facility since 2000. *D.* aff. *albolineatus* were obtained from the pet trade in 2003 and have been maintained as a closed stock in our facility since that time. *Tanichthys albonubes* were obtained from The Wet Spot Tropical Fish (Portland, USA). Fish were reared under standard conditions used to maintain *D. rerio* (~28 °C; 14 L:10D) with larvae initially fed marine rotifers derived from high-density cultures and enriched with Rotimac and Algamac (Reed Mariculture), with older larvae and adults subsequently fed live brine shrimp and a blend of flake foods enriched with dried spirulina, Tetramin and Z-Pro 350 (Zeigler Bros, Inc., USA). Stocks of mutant or transgenic fish included *D. albolineatus*, *rgmb*^{vp67al1}, *rgmb*^{vp67al2}, *runx3*^{vp68a1}, *runx3*^{vp68a2}, *bdh1*^{vp40ac1} and Tg(*aox5:nucEosFP*)^{vp43aTg}; *D. rerio rgmb*^{vp67re1} (refs. [15,41,42]). Developmental staging followed ref. [67], with minor modifications for use in *D. albolineatus*. Unless otherwise specified, male fish were used owing to the sexual dimorphism of *D. albolineatus*.[15] This study was performed in strict accordance with the recommendations in the Guide for the Care and Use of Laboratory Animals of the National Institutes of Health. All animals were handled according to approved institutional Animal Care and Use Committee (ACUC) protocol (#4170) of the University of Virginia. Euthanasia was accomplished by overdose of MS222 followed by physical maceration.

METHOD DETAILS

CRISPR/Cas9 Mutagenesis

CRISPR/Cas9 mutants or F0 mosaics were generated by injecting one-cell stage embryos with approximately 1 nanoliter of 5 μM gRNA:Cas9 RNP complex (IDT, AltR CRISPR/Cas9 reagents), which allowed for highly efficient mutagenesis[68] even in F0 fish. For F0 mosaic analysis, 8 fish with slowed growth or eye defects (observed in the zebrafish mutant *gdf6a*^{vp65re1}) were selected from 46 survivors and genotyped to assess CRISPR/Cas9 mutagenesis efficiency. To produce mutant lines, individual fish were sorted for anal fin phenotypes at juvenile stage and alleles were recovered by intercrossing and outcrossing.

Pharmacological Analysis

LDN-193189 (S2618, Selleck Chem) was used to inhibit BMP signaling. LDN-193189 was dissolved in DMSO (final DMSO concentration 0.5%). In Figures 2B–2D, D. *albolineatus* were treated beginning at 8.5 mm standard length (SL) for a duration of 3 weeks. The concentration of LDN-193189 was set in a gradient of 0, 1 μM, 2 μM, 4 μM, and 12 μM. Control fish received 0.5% DMSO only. In Figure 3B, 8 mm SL *T. albonubes* were treated with either 4 μM LDN-193189 in 0.5% DMSO or 0.5% DMSO alone for 2 weeks. In both experiments, fish were transferred daily into fresh water during the day and fed live brine shrimp, then immersed in freshly prepared drug solutions overnight. For *D. albolineatus*, each treatment group contained 8 fish, except for the 12 μM condition which had 16 fish divided into 2 groups. By the end of the experiment, 1 fish in the 1 μM group, 3 fish in the 4 μM and 8 μM groups, and 8 fish in the 12 μM group died. Brightfield and fluorescence images were collected for the *D. albolineatus* experiment; 1 fish from the 2 μM group was excluded due to sample drift during fluorescence imaging. In the *T. albonubes* experiment, both groups initially contained 9 fish, and 2 fish died in the drug-treated group. For the chronic treatment assay in adult *D. albolineatus*, 4 fish were exposed to 4 μM LDN-193189 in 0.5% DMSO or to 0.5% DMSO alone for 7 days to assess drug efficacy. An additional 12 fish were imaged before and after undergoing the same drug treatment for 25 days. Fish were transferred to fresh water every 3 days to receive a single feeding of live brine shrimp before being returned to newly prepared drug solutions. No mortality occurred during the treatment.

Carotenoid Analyses

Distal (xanthophore-containing) portions of the anal fins from adult *D. albolineatus*, *rgmb*, or *runx3* mutants were dissected and pooled for pigment extraction. 3 biological replicates were prepared, each consisting of 6 fin fragments. 200 μl MilliQ water, 300 μl 200-proof ethanol and 600 μl hexane:tert-butyl methyl ether (hexane:MTBE, 1:1, vol:vol) were added to fish fin samples and mixed by vigorous vortexing. Samples were centrifuged at 12000 g for 5 min, and the supernatants were collected. Extraction was repeated until the fins turned pale. The combined supernatants were dried under nitrogen gas, then saponified with 0.02 M NaOH in ethanol for 4 h. 1 ml saturated NaCl, 2 ml MilliQ water and 2 ml MTBE were added to the saponified extract, then the samples were

Please cite this article in press as: Huang et al., Graded BMP signals modulate yellow and red color in fishes, impacting adult pigment patterns and conspecific shoaling behavior, Current Biology (2026), https://doi.org/10.1016/j.cub.2026.03.007

vortexed and centrifuged at 2000 g in a glass tube. Supernatants were collected and dried under nitrogen gas, before being redissolved in the mobile phase for HPLC analysis. The extracted fish fins were dried and weighed to obtain dry weight measurements. To perform reverse-phase HPLC analysis, carotenoids were dissolved in acetonitrile: methanol: tetrahydrofuran (48:48:4, vol:vol:vol) and injected into an Agilent 1200 series HPLC fitted with a YMC carotenoid column (5.0 μm, 4.6 mm × 250 mm). Samples were then eluted with a gradient mobile phase of acetonitrile:methanol:tetra-hydrofuran (45:45:10, vol:vol:vol) through 9 min, ramping up to acetonitrile:methanol:tetra-hydrofuran (35:35:30) from 9–10 min, followed by isocratic conditions through 12 min, before ramping back down from 12-13 min, followed by isocratic conditions through 15 min. Solvent was pumped at a constant rate of 1.2 mL/min, and the column was maintained at 30°C. Sample elution was monitored using a UV-Vis photodiode array detector at various wavelengths. Carotenoid peaks were identified by comparison to authentic standards of astaxanthin, zeaxanthin, lutein, and dehydro-lutein, as well as their putative *cis* isoforms. Consistent peaks were quantified using three methods: peak area of total signal between 350-600 nm normalized to dry weight; peak area of total signal between 350-600 nm normalized to the combined signal of all peaks; and by absolute quantification using curves generated from authentic standards. We also used fluorescence imaging to measure red vs. yellow carotenoid ratios as described.[15] Briefly, laser intensities for red (excitation wavelength 561 nm) and green (excitation wavelength 488 nm) channels were set to be identical. The ratio of red-to-green signal was quantified to obtain an estimate of the relative of abundance of red vs. yellow carotenoids. For BMP inhibitor experiments, the most distal pigmented cells in the center of the anal fin were imaged. For pSmad immunoreactivity experiments, cells along the 4th fin ray were imaged.

Immunohistochemical Staining

Fins were fixed in 4% paraformaldehyde (PFA) for 1 hour at room temperature and washed 5 times for 5 minutes each with PBST (0.1% Triton X-100 in 1× PBS). Samples were then incubated overnight in blocking solution (2% goat serum in PBST), followed by incubation with a primary antibody against phosphorylated Smad1/5/9 (pSmad; 1:200 dilution, #13820S, Cell Signaling Technology) overnight at 4 °C. After washing 5 times with PBST for 5 minutes each, samples were incubated overnight with a fluorescent dye–conjugated secondary antibody (goat anti-rabbit Alexa Fluor Plus 647, 1:400), washed again, and imaged. Three adult *D. albolineatus* and *T. albonubes* were analyzed. Among the 14 offspring of the *rgmb*$^{vp67re1/+}$ x *rgmb*$^{vp67re1/vp67re1}$ cross, 8 heterozygotes and 6 homozygotes were analyzed.

Lineage Tracing

Photoconversions were performed on *Tg(aox5:nucEos)* fish using a Zeiss LSM 800 laser-scanning confocal microscope equipped with a 405 nm laser and ZEN Blue software. A small rectangular region containing the most distal *nucEos*$^{+}$ cells was photoconverted with 405 nm laser in the anal fin of 9 mm SL larvae. Then fish were treated with 0.5% DMSO, 1 μM LDN-193189 in 0.5% DMSO, or 8 μM LDN-193189 in 0.5% DMSO for 2 weeks (n = 8; no exclusions). Following photoconversion, fish were maintained in tanks shaded from ambient light to prevent spontaneous photoconversion. Final imaging session was performed with fluorescence and then brightfield mode.

Imaging and Image Processing

For the whole fish imaging, fish were euthanized and captured on a Nikon D-810 digital single lens reflex camera with MicroNikkor 105 mm macro lens. Anal fin details were imaged using a Zeiss Axio Observer inverted microscope or Zeiss AxioZoom stereomicroscope equipped with Zeiss Axiocam cameras. Carotenoid autofluorescence was imaged using a Zeiss LSM880 inverted laser confocal microscope in Airyscan SR mode. Images were acquired using a Zeiss AxioObserver inverted microscope equipped with Yokogawa CSU-X1 M5000 laser spinning disk and Hamatsu camera. Images were captured either as single frames or as tiled sets of larger areas that were then stitched computationally using Zeiss ZEN Blue or ZEN Black software. Color balance and display levels were adjusted for entire images as needed and kept consistent across comparisons. Signal intensity and nuclear distance from fin tip were measured using ZEN Black software.

Transmission Electron Microscopy (TEM)

Fins were amputated and pre-fixed for 15–30 min with 4% formaldehyde and 2.5% glutaraldehyde in PBS, then transferred to fresh 4% formaldehyde and 2.5% glutaraldehyde in 100 mM phosphate buffer (pH 7.4) for an additional 2 hr at room temperature. Tissues were post-fixed for 2 hr with 2% osmium tetroxide and 2% uranyl acetate at room temperature, dehydrated in acetone, and flat-embedded in epoxy resin. Embedded blocks were trimmed to create a pyramid shape for ultramicrotomy. Seventy-nanometer sections were cut, collected on carbon mesh grids, and post-stained with lead citrate and Uranyless™. Imaging was performed on an FEI Tecnai F20 equipped with a TEITZ XF416 detector.Bulk RNA-Seq and Single-cell RNA-Seq

Bulk RNA-Seq and Single-cell RNA-Seq

∼100 male *D. albolineatus Tg*(*aox5:nucEosFP*) of 1.5 months old were euthanized. Anal fins were dissected and tissue collected from proximal erythrophore or distal xanthophore regions in PBS and dissociated to cell suspension by Liberase (Roche, Cat# 5401119001) treating at 30 °C for 30 min and filtering through 40 μm strainer. Isolated cells were sorted through Sony SH800 fluorescence activated cell sorter (Sony, Japan). GFP+ healthy cells were collected, and RNA was extracted using RNAqueous™-Micro Total RNA Isolation Kit (Thermo Fisher, Cat# AM1931). Sequencing libraries were constructed using SMART-Seq mRNA LP kit (Takara, Cat# 634768) and sequenced on an Illumina Nextseq-550 using NSQ 500/550 Hi Output KT v2.5 (150

CYS). Reads were aligned to the *Danio albolineatus* genome[14] using Kallisto[62] and analyzed using DESeq2[63] For single-cell RNA-seq, ~150 anal fins were collected from Tg(*aox5:nucEosFP*) fish of 8 mm SL to 14 mm SL and sorted for GFP+ cells. Library production was performed using a Chromium controller (10X Genomics, USA) and Chromium Next GEM Single Cell 3' Kit v3.1 (10X Genomics, USA). Quality control and quantification assays were performed using a Qubit fluorometer (Thermo Fisher, USA) and a 2100 Bioanalyzer (Agilent, USA). We built a zebrafish STAR genome index using Lawson Lab zebrafish transcriptome annotation(58), filtered for protein-coding genes. Final cellular barcodes and Unique Molecular Identifiers (UMIs) were determined using Cell Ranger (10X Genomics, USA). Data were analyzed in Monocle3. In brief, we filtered cells for quality to have less than 5% mitochondrial reads, and greater than 500 unique molecular identifiers and 200 genes expressed. RNA-seq data are available through SRA (accession ID: PRJNA1365945). We used Uniform Manifold Approximation and Projection (UMAP) to project transcriptomic space in two dimensions followed by Louvain clustering. We assigned clusters to cell types by comparing genes detected to published cell type specific markers. Cell type marker analysis, differential expression and trajectory analyses used standard methods and functions as described (cole-trapnelllab.github.io/monocle3/docs/). Gene module identification was performed using Monocle3 find_gene_modules() across clusters. To assess gene expression enrichment across biological, molecular and cellular functions with bulk mRNA-Seq data, we used WebGestalt 2024 (https://www.webgestalt.org/)[69] for over-representation analyses with gene ontology terms and KEGG pathways, We additionally tested for enrichments in transcript abundance for major signaling pathways and genes involved in carotenoid or pteridine pigmentation, using Fisher's Exact tests in R v4.5.2 with lists of genes that we compiled to include core pathway components (e.g., encoding ligands, receptors and co-receptors and downstream effectors of signaling pathways) as well as transcriptional regulators that have often been found immediately upstream or downstream of these pathways (e.g., Msx genes of BMP signaling); individual genes were considered differentially expressed in these pathways if observed $\log_2$ fold-change > |0.5| with adjusted *P*-value < 0.05. Genes of the *D. albolineatus* genome, assigned gene symbols for presumptive orthologues of zebrafish where possible (see below), were prefiltered prior to analysis to include only protein-coding loci (*n*=16,143). Finally, because little is known of erythrophores compared to other pigment cell types, we also compiled differentially expressed genes of erythrophores and xanthophores relative to a curated list of genes known to have pigmentary roles across major vertebrate model organisms.[70] Gene sets and classifications (enriched in erythrophores, xanthophores, or neither) are provided in Data S1B.

Genome Assembly and Annotation

For assessing standing genetic variation in fin phenotype, we generated a high quality *de novo* genome assembly for *D. albolineatus* using PacBio sequencing. High-fidelity (HiFi) reads were generated from a single male (ZZ) individual of *D. albolineatus*. Raw sequencing reads in BAM format were filtered to retain only those with a quality score (Read Quality, RQ) greater than Q20 (RQ >= 0.99) using bamtools.[71] The filtered BAM files were then merged and converted to FASTQ format using pbindex and bam2fastq (PacBio SMRT Tools). Read quality was assessed using NanoPlot[72]. The pre-processed HiFi reads were assembled *de novo* using Hifiasm (v0.19-r320)[73] with default parameters. The resulting primary contig assembly (*.bp.p_ctg.gfa) was extracted and converted to FASTA format using awk.

The initial *de novo* assembly was assessed for completeness using QUAST (v5.0.2)[74] and BUSCO (v5.4.3)[75] with the Actinopterygii lineage dataset. To improve the contiguity and order the contigs into chromosome-scale scaffolds, the assembly was polished and scaffolded using RagTag (v2.1.0).[76] Given the conservation of karyotype number across *Danio*, the high-quality, chromosome-level assembly of the reference species, *Danio rerio* (NCBI GCF_000002035.6, GRCz11),[77] was used as the reference guide for scaffolding. Repetitive elements were identified and masked in a multi-step procedure. First, repeats were identified *de novo* using RepeatModeler (v2.0.4)[78] on the scaffolded genome to build a custom repeat library. The assembly was then masked in three iterative rounds using RepeatMasker (v4.1.2)[79]: 1. Simple Repeats: Masking for simple repeats and low-complexity regions using the NCBI standard and *Danio* species parameters, with output converted to GFF3 format using a custom script; 2. Known Repeats: Masking against known repeats from *Danio* species using the RepeatMasker database[80]; 3. *De Novo* Repeats: Masking using the custom repeat library generated by RepeatModeler. The results from all three masking runs were concatenated, and the final soft-masked genome FASTA file was generated using bedtools maskfasta[81] with the combined GFF3 file.

Gene annotation was performed by lifting over a robust annotation from the closely related *Danio rerio* reference genome. We used Liftoff (v1.6.3)[82] to project the gene annotations from *Danio rerio* (GRCz11, NCBI GCF_000002035.6 GTF file) onto the newly assembled and scaffolded *D. albolineatus* genome. This approach leveraged the well-curated annotation of *D. rerio* to provide functional gene models for the novel assembly.

Bulk Segregant Analysis

Loci contributing to anal fin color and pattern were mapped using a Bulk Segregant approach comparing two distinct F2 pools with 23 male specimens each derived from an original cross between a female *D. albolineatus* (yellow and red anal fin) and a male *D. aff. albolineatus*[12,27] (red anal fin). The two pools, representing fish resembling either *D. albolineatus* or *D. aff. albolineatus* were sequenced to a mean coverage of 2x the number of specimens. Raw Illumina PE 150bp sequencing reads were quality-trimmed and filtered using fastp (v0.23.2).[83] The cleaned paired-end reads were aligned to the final soft-masked *D. albolineatus* reference genome (RagTag-scaffolded with *D. rerio*) using Bowtie 2 (v2.4.5)[84] with the -sensitive-local preset. The resulting alignments were filtered to remove unaligned reads and reads with low mapping quality (MAPQ < 20) using Samtools (v1.17)[85] Duplicate reads were identified and removed using a series of steps involving samtools fixmate and samtools markdup to ensure unbiased variant calling. Single-nucleotide polymorphisms (SNPs) were called across all samples using BCFtools' mpileup (v1.17)[85] in a per-region,

Please cite this article in press as: Huang et al., Graded BMP signals modulate yellow and red color in fishes, impacting adult pigment patterns and conspecific shoaling behavior, Current Biology (2026), https://doi.org/10.1016/j.cub.2026.03.007

parallelized workflow. The mpileup and call commands were executed with the –multiallelic-caller option, annotating for allelic depth (AD) and total depth (DP).

Variants were filtered based on quality (QUAL >= 20), mapping quality (MQ >= 20), and minimum per-sample read depth (MIN(FMT/DP) >= 5). Two distinct filtered VCF sets were generated: 1. Population Genetics Filter (PopGen): Used the base quality and depth filters defined above; 2. Association Filter: Used the PopGen filters and included an additional filter for minor allele frequency (MAF) to retain only common variants (MAF >= 0.05 and MAF <= 0.95). The association between genetic variants and the pooled phenotypes was assessed using two independent methods: 1. Allele Frequency Comparison: The PopGen VCF files were converted to Popoolation2 (v1.201)[86] sync format for allele frequency comparison. The Popoolation2 (v1.201) fisher-test.pl script was employed to calculate Fisher's Exact Test P-values for allele frequency differences between pools at each SNP, implementing a dynamic coverage filter based on the interquartile range (IQR) of 10kbp window depth values (Q3 + 5 * IQR) to remove outliers; 2. Sliding Window Analysis: The Association VCF files were reformatted and analyzed using the QTLseqr R package (v2.1.0).[87] This analysis calculates the tricubed deltaSNP (allele frequency difference) and the G' statistic[88] in 1 Mbp sliding windows with 100 kb steps. By calculating a distance-weighted average of G statistics for neighboring SNPs, this method accounts for linkage disequilibrium and reduces noise inherent in individual SNP calling. Significant QTL were identified using a Benjamini-Hochberg[89] false discovery rate (q <= 0.05) based on a log-normal null distribution of G' values. Furthermore, by identifying fixed allelic differences between parental F0 *D. albolineatus* and *D. aff. albolineatus*, we phased the deltaSNP statistic such that *D. albolineatus* alleles are represented by positive values.

To identify the most robust candidate single-nucleotide polymorphisms (SNPs) underlying the caudal fin color, we implemented a three-tiered prioritization strategy: 1. Statistical Cross-Reference: Significant loci were defined by intersecting the outputs of both QTL mapping methods. Only SNPs falling within a genomic region identified by QTLseqr as significant (q-value <= 0.05) and having a Fisher's Exact Test P-value greater than the 99.9th percentile threshold calculated by Popoolation2 were retained; 2. Parental Genotype Filtering: The resulting subset was further filtered using the fixed-genotype calls from the Grandparent samples. This stringent filter retained only SNPs that adhered to a model of Parental Fixed Difference (PfixedDiff), where the two grandparental lineages were fixed for opposing alleles (0/0 vs. 1/1). This step maximized the chance of identifying a true causal variant segregating in the F2 pools; 3. Functional Annotation: The final list of candidate SNPs was functionally annotated using SnpEff (v4.3t),[90] employing the *D. rerio* lifted gene annotation to predict the potential molecular consequence (e.g., missense, nonsense, intron variant) of each variant. Nucleotide diversity (pi), Tajima's D,[91] and Weir and Cockerham's F_{st} were calculated for the pools using grenedalf (v0.6.1)[92] from the PopGen-filtered VCF set in non-overlapping 10 kbp windows.

SHOALING PREFERENCE ASSAY

To test for a social aggregative behavioral preference for different phenotypes, wild-type *D. albolineatus*, red mutant *rgmb*^{vp67re1} and yellow mutant *bdh1a*^{vp40ac1} were used. All individuals were 1 year old and selected for comparable size and body shape. The behavioral arena consisted of a glass tank (51 × 28 × 25 cm) with bottom covered by small gravel to simulate a natural environment. Two identical glass chambers designated as male compartments (12 × 8 × 12 cm) were placed at opposite ends of the tank. These were connected by two transparent Plexiglas boards to create a female compartment (21 × 12 × 12 cm) that allowed the test female to swim freely between male chambers. The glass tank and all chambers were filled with system water to a depth of 12 cm. The arena was enclosed in a white-cloth-covered box (1 × 1 × 1 m) to diffuse light and minimize external visual disturbances. Full-spectrum LED lights (Draco Broadcast Dracast LED500, 5600 K) were positioned 1 m above the tank on both sides outside of the box to ensure uniform illumination. A front opening allowed the camera lens for video recording. All trials were recorded at 30 frames per second using a Panasonic HC-V770 digital camera. Two black dividers were placed on either side of the female compartment during setup. Two male fish were introduced into the male chambers and one female into the central compartment, each using separate fish nets. Male chambers were covered with transparent lids to prevent escape. Fish were acclimated for 10 min before testing. Testing began upon simultaneous removal of the dividers, and each assay lasted at least 5 min. After testing, fish were removed, and chambers were rinsed with RO water before the next trial. Each fish was used only once. To control for circadian effects on sensory behavior and motivation, all assays were performed between 08:30 and 11:30. The positions of the male genotypes were alternated between trials to avoid positional bias. Trials were excluded if the female showed no apparent interest in either male (i.e., swam continuously without spending more than 10 seconds near either male chamber). n =16 fish in wild-type vs. yellow trials (20 in total, 4 excluded); n =17 fish in red vs. yellow trials (20 in total, 3 excluded); n =14 fish in wild-type vs. red trials (17 in total, 3 excluded). The female's horizontal distance from the chamber center was measured every 15 frames (0.5 s).

QUANTIFICATION AND STATISTICAL ANALYSES

Analyses of quantitative data were performed in JMP Pro 18 (SAS Institute, Cary, NC) or in R v4.5.2, with transformations applied as noted in figure legends to correct for heterogenous variances in residuals as warranted. Figure legends or panels indicate tests used, values of test statistics, parameter estimates, sample sizes (individual animals, cells or both depending on analysis), definitions of centers dispersion and precision measures displayed in plots, or, in some instances, point to analytical details as provided in Data S1.

Current Biology, Volume *36*

Supplemental Information

Graded BMP signals modulate yellow and red color in fishes, impacting adult pigment patterns and conspecific shoaling behavior

Delai Huang, Pietro L.H. de Mello, Tiffany Liu, Yu Liu, Emaan H. Kapadia, Yipeng Liang, Jianguo Lu, Joseph C. Corbo, and David M. Parichy

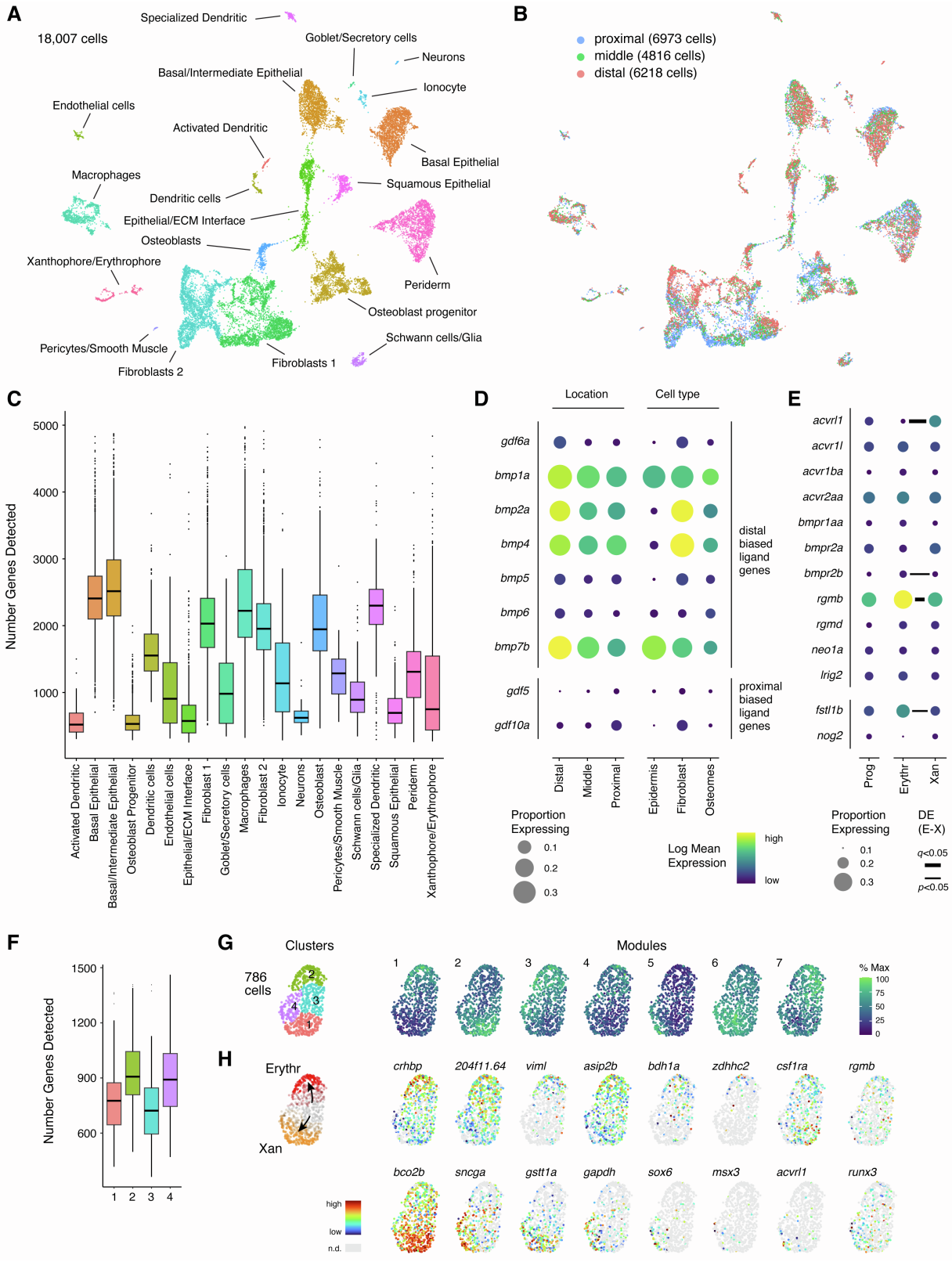
A
18,007 cells
Specialized Dendritic
Goblet/Secretory cells
Neurons
Basal/Intermediate Epithelial
Ionocyte
Endothelial cells
Activated Dendritic
Basal Epithelial
Macrophages
Squamous Epithelial
Dendritic cells
Epithelial/ECM Interface
Osteoblasts
Xanthophore/Erythrophore
Periderm
Osteoblast progenitor
Schwann cells/Glia
Pericytes/Smooth Muscle
Fibroblasts 1
Fibroblasts 2
B
proximal (6973 cells)
middle (4816 cells)
distal (6218 cells)
C
Number Genes Detected
5000
4000
3000
2000
1000
Activated Dendritic
Basal Epithelial
Basal/Intermediate Epithelial
Osteoblast Progenitor
Dendritic cells
Endothelial cells
Epithelial/ECM Interface
Fibroblast 1
Goblet/Secretory cells
Macrophages
Fibroblast 2
Ionocyte
Neurons
Osteoblast
Pericytes/Smooth Muscle
Schwann cells/Glia
Specialized Dendritic
Squamous Epithelial
Periderm
Xanthophore/Erythrophore
D
Location
Cell type
gdf6a
bmp1a
bmp2a
bmp4
bmp5
bmp6
bmp7b
gdf5
gdf10a
distal biased ligand genes
proximal biased ligand genes
Distal
Middle
Proximal
Epidermis
Fibroblast
Osteomes
Proportion Expressing
0.1
0.2
0.3
Log Mean Expression
high
low
E
acvrl1
acvr1l
acvr1ba
acvr2aa
bmpr1aa
bmpr2a
bmpr2b
rgmb
rgmd
neo1a
lrig2
fstl1b
nog2
Prog
Erythr
Xan
Proportion Expressing
0.1
0.2
0.3
DE (E-X)
q<0.05
p<0.05
F
Number Genes Detected
1500
1200
900
600
1
2
3
4
G
Clusters
786 cells
2
3
4
1
Modules
1
2
3
4
5
6
7
% Max
100
75
50
25
0
H
Erythr
Xan
high
low
n.d.
crhbp
204f11.64
viml
asip2b
bdh1a
zdhhc2
csf1ra
rgmb
bco2b
sncga
gstt1a
gapdh
sox6
msx3
acvrl1
runx3

Figure S1. Transcriptomic analyses reveal differential expression of BMP ligand genes in fin tissue environment and modules of gene expression associated with xanthophore and erythrophore differentiation. Related to Figure 1.

(A–D) Results for cells isolated from proximal, middle and distal regions of wild-type anal fins at ~12 mm standard length (SL) for 10X Chromium single cell RNA-sequencing (scRNA-Seq), subsetted for resident cells rather than circulating erythroid and immune cells (18,007 of 24,358 cell total).

(A, B) Cluster cell type assignments and relative contributions of proximodistal cell origins, respectively.

(C) Numbers of genes detected were variable across cell types, possibly reflecting different efficiencies of transcript recovery due to fragility of some cell morphologies. Boxes, medians with IQR, lines extend to 1.5x IQR with outlier cells displayed as individual values.

(D) BMP ligand genes were differentially expressed proximodistally and across cell types in the local tissue environment of pigment cells (cell types shown aggregate clusters representing basal cells of epidermis, dermal fibroblasts, and mesenchymal osteoblast progenitors and osteoblasts; 11,216 cells total). Preliminary analyses did not reveal significant interactions for anatomical location and cell type affecting gene expression.

(E–H) Results for pigment cells and progenitors isolated by fluorescence activated sorting of *aox5*:nucEos-expressing[S1] cells from anal fins of 8–14 mm SL larvae for 10X Chromium scRNA-Seq.

(E) Transcripts for canonical and non-canonical BMP receptors as well as secreted inhibitors of BMP signaling were evident amongst *aox5*+ cells representing unpigmented progenitors, erythrophores and xanthophores. Expression levels were assessed between erythrophores and xanthophores with significance levels of differences indicated by horizontal bars as determined in Monocle3.

(F) Numbers of genes detected among clusters of *aox5*+ cells. Boxplot as in Figure S1C.

(G) Four clusters of *aox5*+ cells were detected with expression levels shown for each of 7 modules of co-expressed genes in UMAP space.

(H) Inspection of cluster-specific and module-specific gene expression (Data S1F,G), and comparison with results of bulk mRNA-Seq for mature cells (Data S1A) indicated that clusters 1 and 2 represented xanthophores and erythrophores respectively, whereas clusters 3 and 4 were more likely to represent orange-pigmented[1] or unpigmented cells not yet committed to either sublineage. Examples of some informative genes are mapped onto UMAP space.

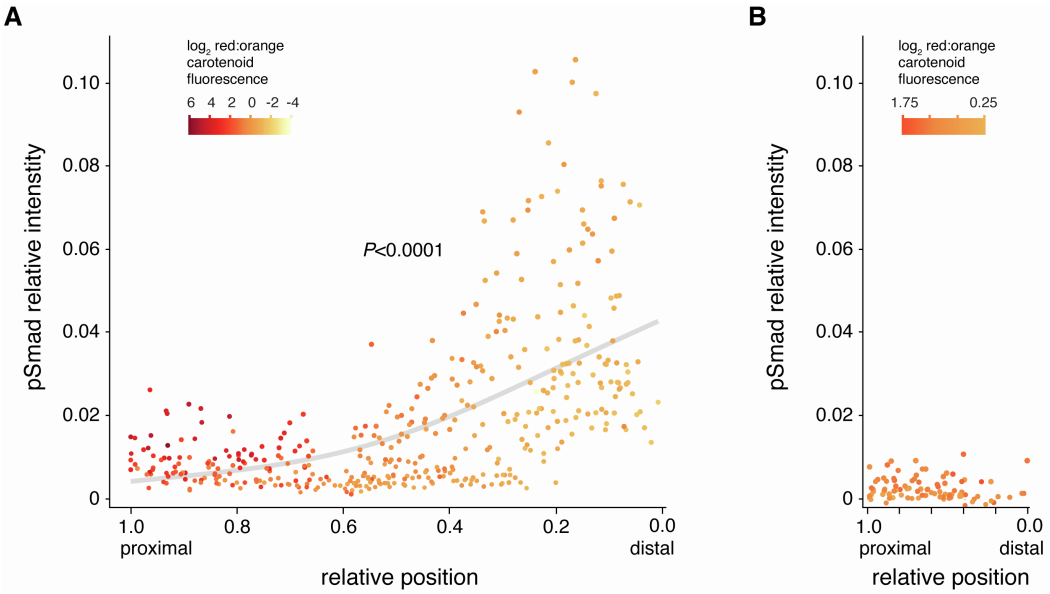

Figure S2. Graded BMP signal reception across the fin revealed by pSmad immunoreactivity. Related to Figure 2.

(A) Nuclear pSmad immunoreactivity relative to Dapi fluorescence in ~15 mm SL fish when erythrophores and xanthophores have differentiated with differences evident in red-to-orange carotenoid fluorescence ratios (n=3 wild-type fish, 421 cells). pSmad immunoreactivity was significantly greater distally, among xanthophores, than proximally where erythrophores predominated (curve fit slope = -0.11, quadratic = 0.07; both parameters P<0.001). Positions are relative to most proximal and distal cells assessed.

(B) At ~8.5 mm SL only progenitors to erythrophores and xanthophores of intermediate color are present[S1] and no gradient in pSmad immunoreactivity was evident (quadratic and linear models, both P>0.15; n=3 fish, 90 cells). Plot widths in A and B are proportional to proximal–distal fin lengths at the two stages shown.

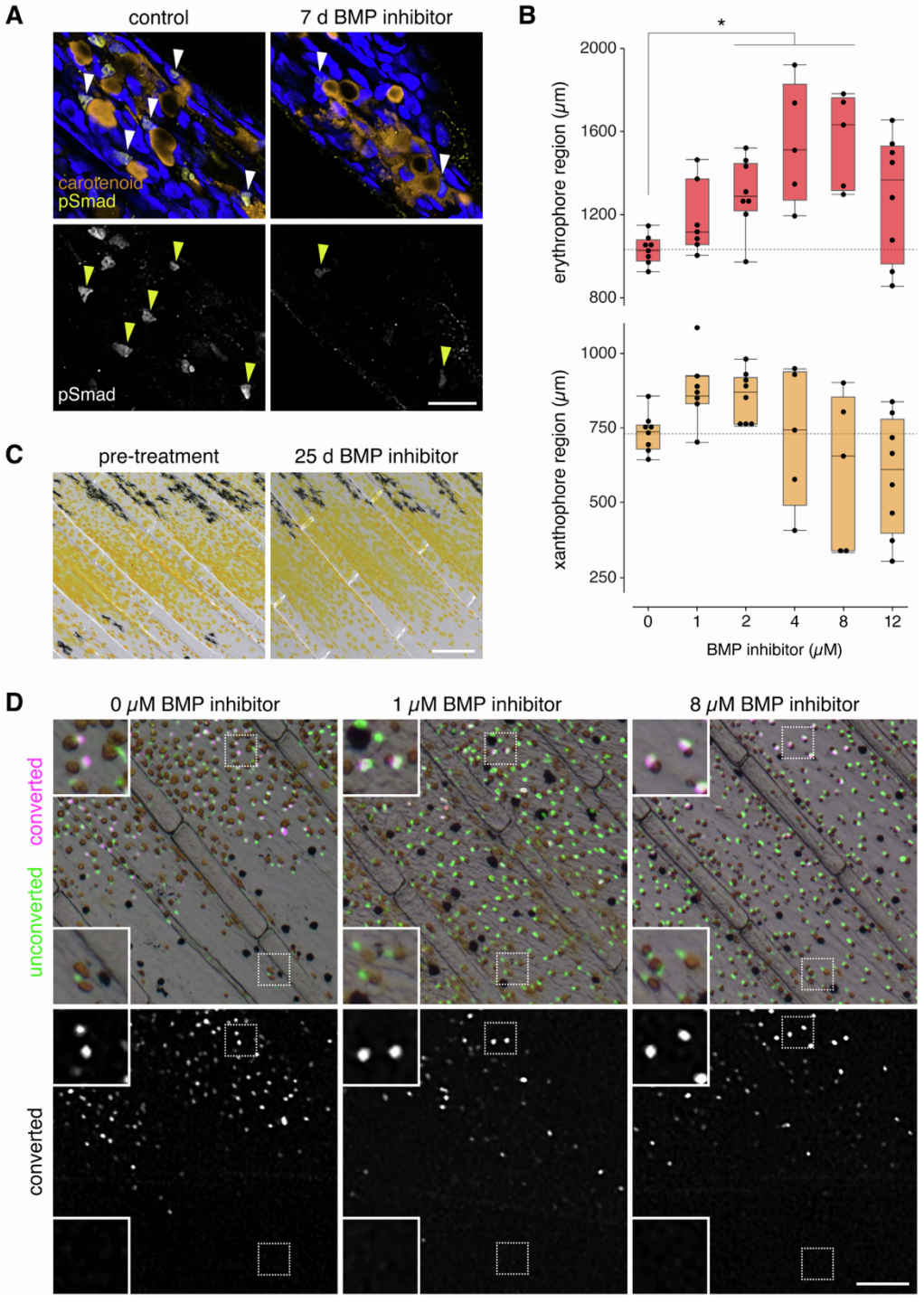
A
control
7 d BMP inhibitor
carotenoid
pSmad
pSmad
B
*
erythrophore region (μm)
2000
1600
1200
800
xanthophore region (μm)
1000
750
500
250
0
1
2
4
8
12
BMP inhibitor (μM)
C
pre-treatment
25 d BMP inhibitor
D
0 μM BMP inhibitor
1 μM BMP inhibitor
8 μM BMP inhibitor
converted
unconverted
converted

Figure S3 BMP signal attenuation affected differentiation. Related to Figure 2.

(A) pSmad immunoreactivity was pronounced in nuclei of xanthophores at the distal portion of the fin, yet BMP inhibitor markedly attenuated this staining. Arrowheads show examples of nuclei adjacent to carotenoid accumulations with either strong immunostaining (control) or weak immunostaining (7d BMP inhibitor). Orange, xanthophore carotenoid autofluorescence; yellow, pSmad staining; blue, Dapi.

(B) Regions covered by erythrophores and xanthophores were altered by BMP inhibitor treatment, as measured by proximal–distal distances populated by these cells at the fifth fin ray. BMP inhibition led to significantly larger regions covered by erythrophores (treated vs. control, contrast $F_{1,35}$=16.8, P=0.0002; *post-hoc* means comparisons to control: *, Dunnet's test P<0.05; overall ANOVA $F_{5,35}$=5.2, P=0.0011). Regions covered by xanthophores varied with treatment (overall ANOVA $F_{5,35}$=3.9, P=0.0066) but could be greater than controls, particularly at low inhibitor doses, or less than controls at high doses. Inhibitor treatment also led to significantly increased variability in coverage by erythrophores and xanthophores (Levene's tests P=0.0073, P=0.0009, respectively), leading to heteroscedasticity in residuals, adequately corrected for parametric analyses by reciprocal transformation (erythrophore regions) and square transformation (xanthophore regions). Boxes, medians with IQR, bars extend to 1.5x IQR, superimposed on values representing regions of individual fish.

(C) Xanthophores that had already developed in older fish were similarly abundant before treatment and after 25 d of BMP inhibitor treatment, suggesting xanthophores do not die as a consequence of BMP signaling inhibition.

(D) Fate mapping with photoconvertible fluorophore expressed by xanthophores and erythrophores (*aox5*:nucEosFP) showed that cells marked by photoconversion (green → red, shown here in magenta for visual accessibility) early in pattern development and fin outgrowth did not migrate to distal regions where control fish have very few carotenoid-containing pigment cells (0 μM), fish with low doses of inhibitor developed xanthophores (1 μM) and fish with high doses (8 μM) developed erythrophores. Presence of only unconverted green fluorophore in distal regions further indicated that cells had not yet started to express *aox5*:EosFP and so had differentiated from unspecified progenitors, likewise excluding the possibility of transdifferentiation, which has been documented unidirectionally (erythrophores → xanthophores) during regeneration[S1]. Upper panels show brightfield images superimposed on fluorescence of unconverted fluorophore and converted fluorophore. Continued expression of *aox5*:nucEosFP after conversion leads to all cells having unconverted fluorophore and appearing white (green+magenta) except where live specimen movement during acquisition led to channel offset.

Scale bars, 20 μm (A), 200 μm (C), 100 μm (D).

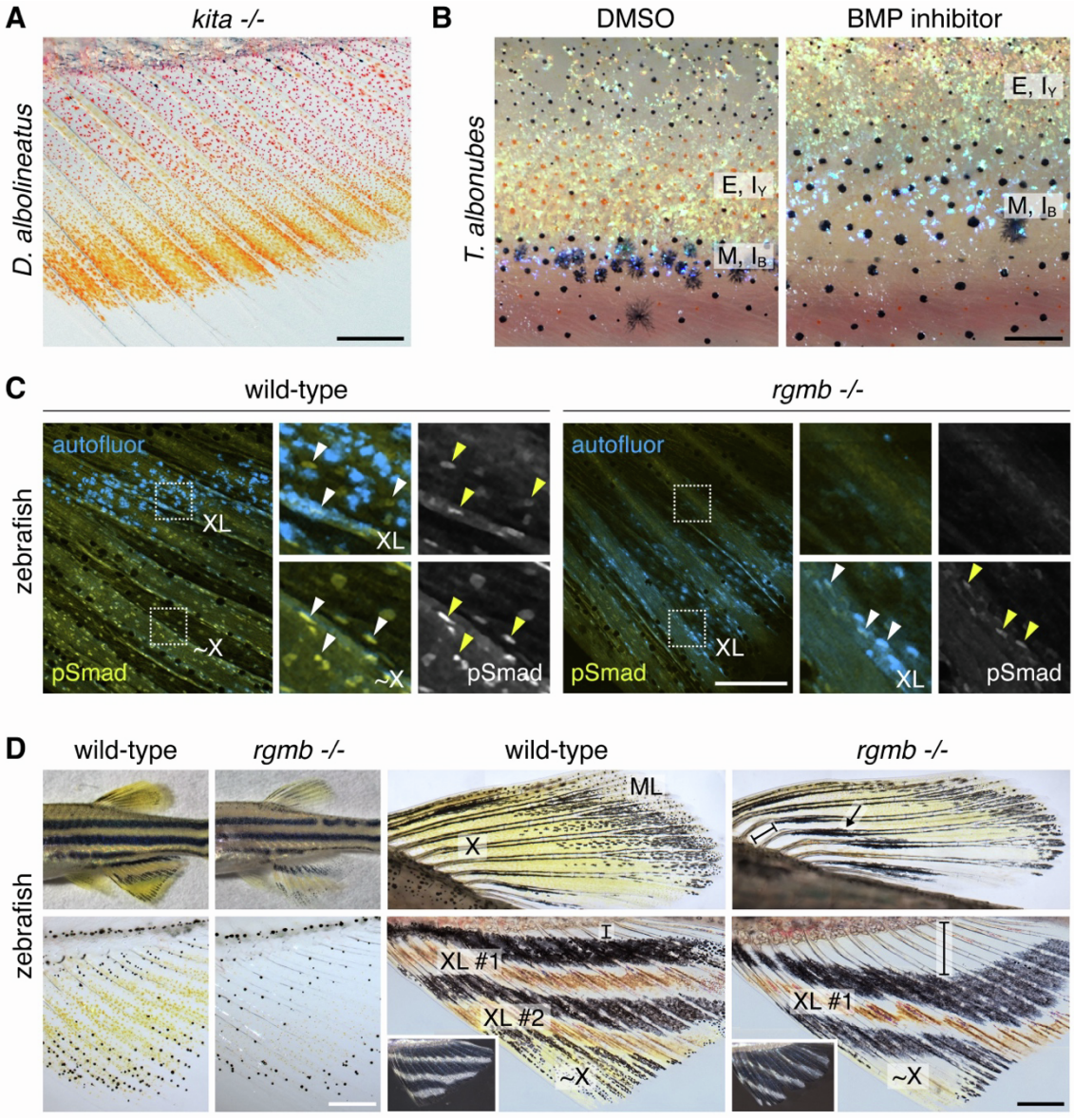
A
kita -/-
D. albolineatus
B
DMSO
BMP inhibitor
T. albonubes
E, IY
M, IB
E, IY
M, IB
C
wild-type
rgmb -/-
zebrafish
autofluor
XL
~X
pSmad
autofluor
XL
pSmad
XL
pSmad
D
wild-type
rgmb -/-
wild-type
rgmb -/-
zebrafish
ML
X
XL #1
XL #2
~X
XL #1
~X

Figure S4. Additional roles for BMP signals in setting pattern phenotype. Related to Figures 2, 3.

(A) In *D. albolineatus*, neither the proximal boundary between erythrophores and xanthophores nor the distal boundary of xanthophores depended on melanophores normally at these locations, as shown here in a mutant for the Kit receptor tyrosine kinase encoded by *kita*, which lacks anal fin melanophores due to an autonomous requirement for Kit in this lineage[S2,S3]. Compare with Figure 1A.

(B) A BMP requirement for body pigment pattern of *T. albonubes* was revealed by inhibitor-treated fish, in which regions of erythrophores and yellow iridophores (E, I_Y) and melanophores and blue iridophores (M, I_B) were shifted dorsally in comparison to controls. Yellow and blue iridophore morphologies and arrangements resembled those of zebrafish interstripes and stripes, respectively.[S4]

(C) In wild-type zebrafish, xantholeucophores (XL) were only weakly pSmad+ (autofluorescing pigmentary contents adjacent to pSmad+ nuclei), whereas more distal xanthophore-like cells (~X) were strongly pSmad+. In the *rgmb* mutant, xantholeucophores were shifted distally and pSmad immunoreactivity was reduced overall.

(D) In comparison to the wild type, *rgmb* mutants had moderately more frequent stripe breaks and reduced yellow pigmentation (upper left; ~13.5 mm SL) and xanthophores in the fins were markedly delayed in their differentiation (lower left; ~9 mm SL). In dorsal fins of young adults (~3 months old), a pigment-cell free region (bracket) and ectopic melanophore stripe were present where xanthophores (X) occurred in wild-type; melanoleucophores (ML) were markedly fewer[S5]. In anal fins, the first developing interstripe of xantholeucophores (XL #1) was present distal to the corresponding interstripe of wild-type and a larger pigment-cell free region was evident proximally (brackets). In older *rgmb* mutants additional interstripes eventually formed, with angled or irregular patterns (insets, ~8 months old.

Scale bars, 500 μm (A), 200 μm (B,C), 2 mm (D upper left), 250 μm (D lower left), 500 μm (D right).

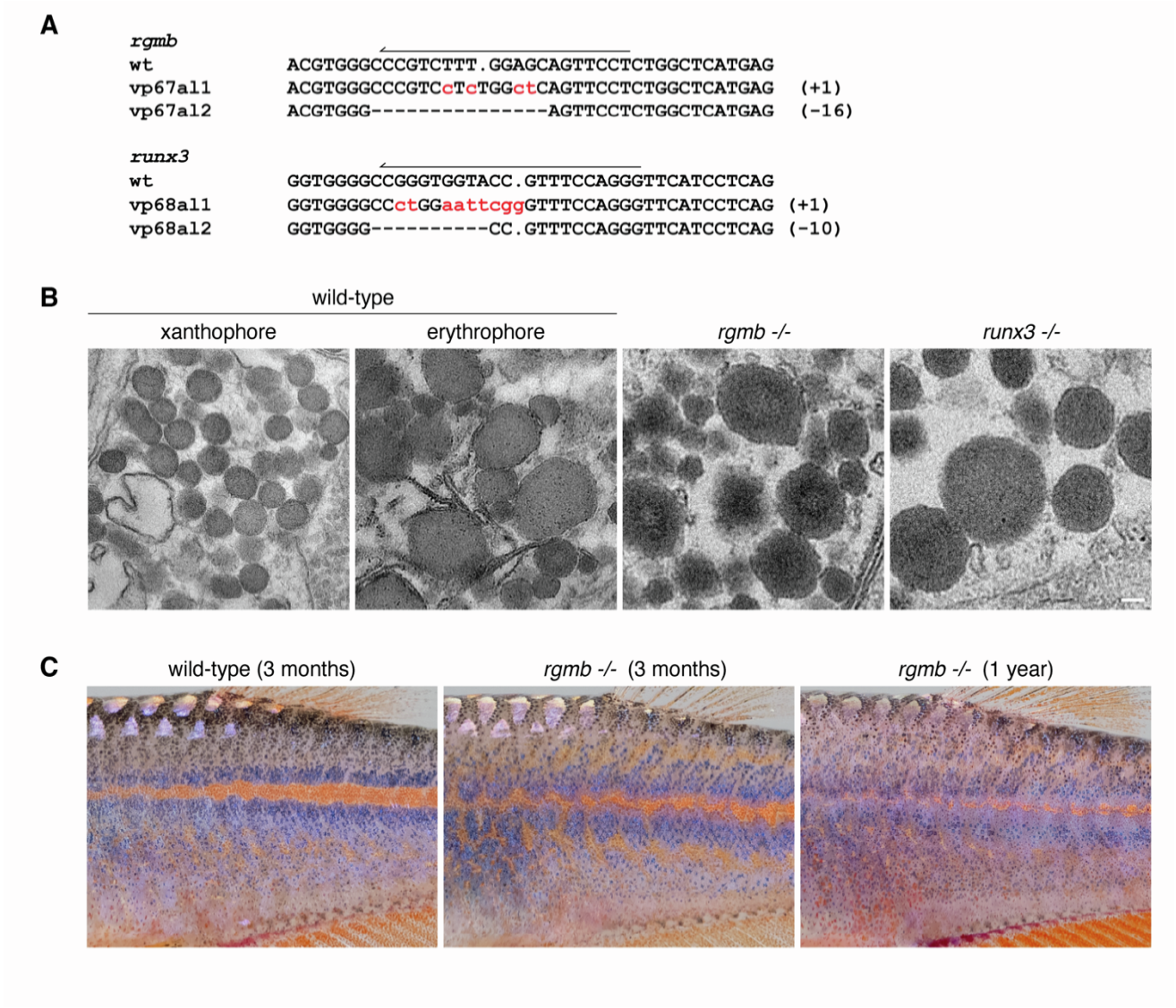

Figure S5. Mutants for *rgmb* and *runx3* of *D. albolineatus*. Related to Figure 4.

(A) Frameshift alleles recovered following CRISPR/Cas9 targeting that that led to premature termination codons; differences in phenotype were not evident across alleles. Arrows indicate CRISPR target sites in wild-type with numbers at right showing total numbers of base pairs inserted or deleted.

(B) Transmission electron microscopy showing electron-dense carotenoid vesicles of fin distal xanthophores and proximal erythrophores in wild-type as well as ectopic distal erythrophores in *rgmb* and *runx3* mutants. Vesicles of mutant cells were of similar size to those of erythrophores in wild-type, which were consistently larger than those of xanthophores.

(C) Body pigmentation of *rgmb* mutants differed from wild-type in having a somewhat less distinctive and more irregular pattern of already weak melanophore stripes and light interstripe. During later development the pattern of wild-type was maintained whereas an increasingly diffuse pattern emerged in *rgmb* mutants. Image of 1-year fish is re-scaled to 75% of original size to illustrate an anatomical region comparable to that of 3-month fish).

Scale bar, (B) 100 nm.

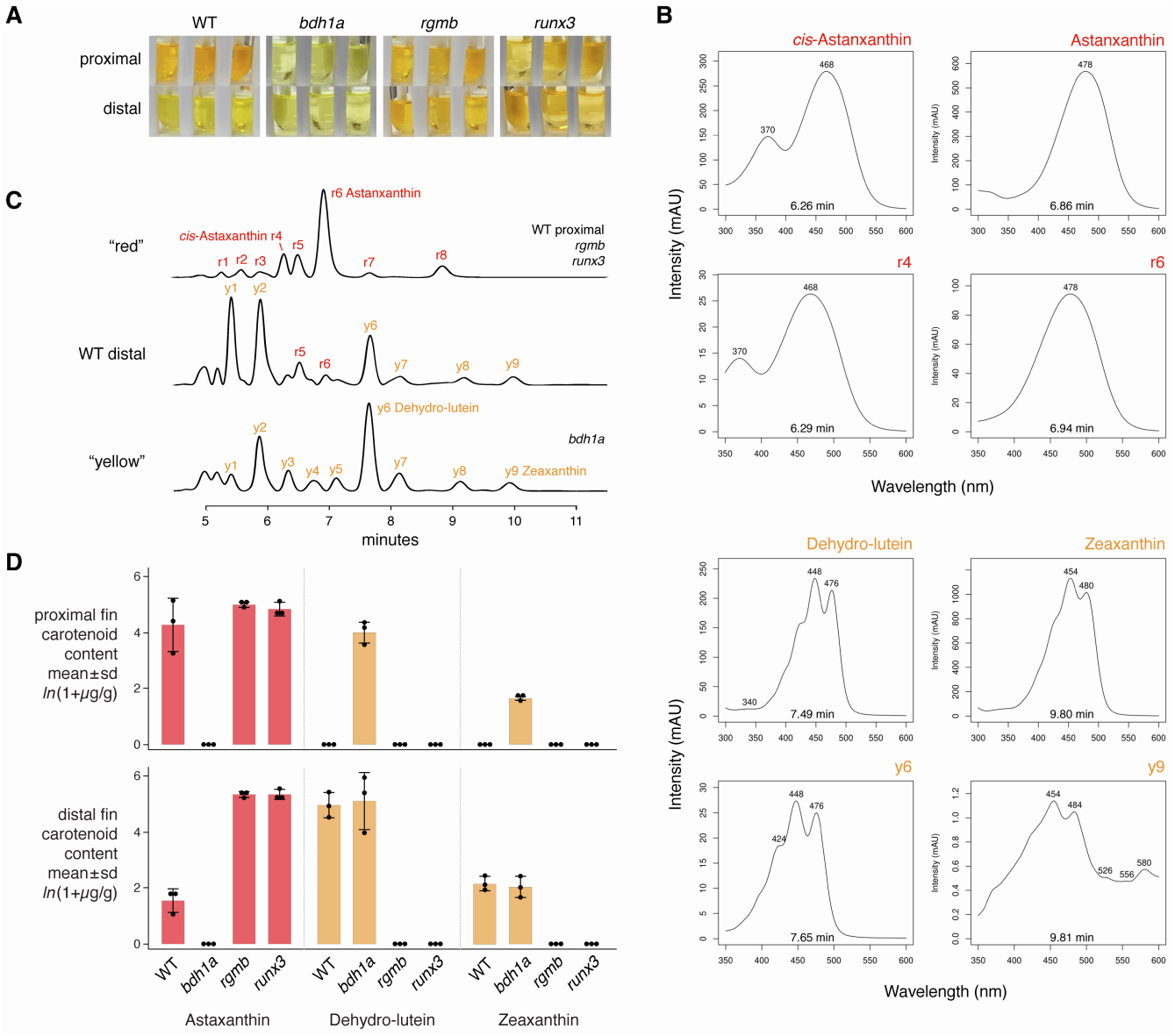

Figure S6. Chemical analysis of carotenoid contents. Related to Figure 4.

(A) Color differences were evident during extraction of carotenoids from proximal and distal fin regions of wild-type but not mutants. Each anatomical pair of samples represents fin tissue pooled from 6 individual fish.

(B) Standards for carotenoids (red: *cis*-Astaxanthan, Astaxanthan; yellow: Dehydro-lutein, Zeaxanthin) above inferred corresponding peaks from red or yellow tissue in C.

(C) Example chromatograms of exclusively red or yellow tissue (representative of genotypes and region shown at right), along with distal tissue of wild-type with inferred unique and overlapping peaks numbered.

(D) Quantification of tissue contents for identified carotenoids (ANOVA genotype x position interactions all $F_{3,16}$>23, P<0.0001 after *ln*-transformation). Shown are means with error bars spanning ±1 standard deviation superimposed on estimates for individual samples collected as described in Methods; see Data S1H.

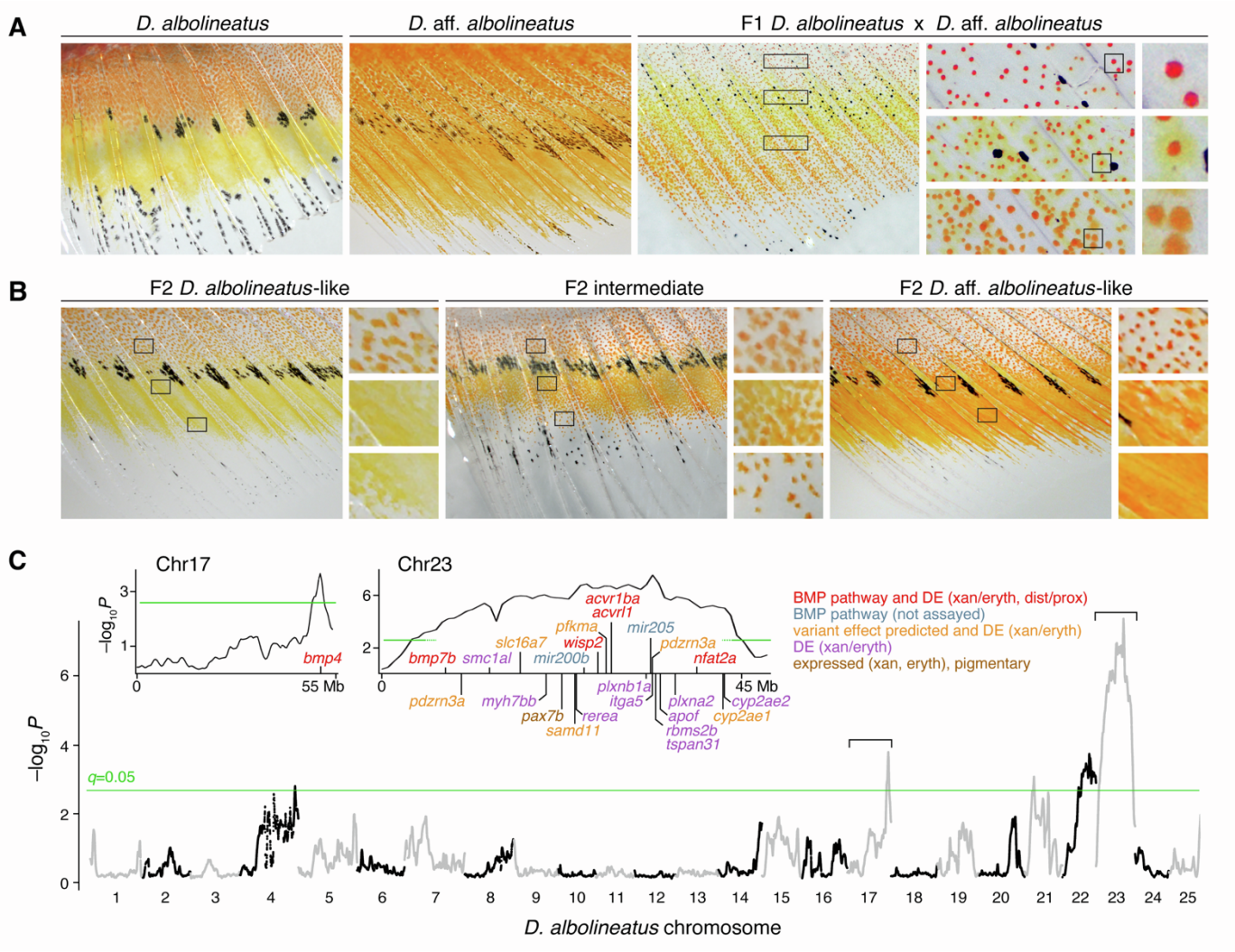
A
D. albolineatus
D. aff. albolineatus
F1 D. albolineatus x D. aff. albolineatus
B
F2 D. albolineatus-like
F2 intermediate
F2 D. aff. albolineatus-like
C
Chr17
Chr23
bmp4
55 Mb
acvr1ba
acvrl1
pfkma
mir205
slc16a7
wisp2
pdzrn3a
bmp7b
smc1al
mir200b
nfat2a
pdzrn3a
myh7bb
pax7b
samd11
rerea
plxnb1a
itga5
plxna2
apof
cyp2ae2
cyp2ae1
rbms2b
tspan31
BMP pathway and DE (xan/eryth, dist/prox)
BMP pathway (not assayed)
variant effect predicted and DE (xan/eryth)
DE (xan/eryth)
expressed (xan, eryth), pigmentary
−log10P
q=0.05
D. albolineatus chromosome

Figure S7. Fin pattern variation in *D.* aff. *albolineatus*, *D. albolineatus* and related taxa. Related to Figure 4.

(A) Phenotypes of fish used in genetic mapping, showing males of parental strains *D. albolineatus* and *D.* aff. *albolineatus*, along with fin pattern of the F1 male, and examples of F2 progeny. In contrast to *D. albolineatus*, anal fins of *D.* aff. *albolineatus* have erythrophores that extend further distally and lack xanthophores. F1 progeny had overall reddish coloration proximally, yellow–orange in middle regions, and orange coloration distally. These phenotypes resulted from different colors within individual cells, especially in the middle of the fin, with prominent concentrations of red carotenoids following epinephrine treatment as well as a widely dispersed yellow pigment. The latter pigment may represent aberrantly localized carotenoids or yellow pteridines expressed in *D.* aff. *albolineatus* or uniquely in the hybrid; *D. albolineatus* xanthophores and erythrophores have pteridines that are colorless to the human eye[1] but fin chromatophores of other species have both colorless and yellow pteridines, with the latter accumulating at the expense of the former in certain genetic backgrounds[S6].

(B) Across ~300 F2 progeny including ~150 male individuals of a single family, pigmentary phenotypes ranged across a continuum from those closely resembling *D. albolineatus* (left), through intermediate states (middle), to those closely resembling *D.* aff. *albolineatus* (right).

(C) Genetic mapping for variation in fin pattern and color revealed multiple regions of association across the genome, including one end of Chr17 and a strong nearly chromosome-wide association with Chr23 (insets; Data S1I-1). Broad peaks of this sort could indicate structural changes (e.g., inversions) that suppress recombination, reduced recombination for that chromosome generally, natural selection or artificial selection affecting multiple loci (e.g. in the pet trade, from which which *D.* aff. *albolineatus* is derived), or some combination of these factors. Plots show smoothed $-\log_{10}(P\text{-values})$ calculated with QTLSeqR (green lines, q=0.01). Candidate genes: in red, associated with BMP signaling and differentially expressed (DE) between erythrophores and xanthophores or between distal-to-proximal fin regions of *D. albolineatus* (Figure 1C,D, Figure S1D,E); in blue, modulators of BMP signaling; in orange, having coding sequence variants (Data S1I-2) predicted to impact function and DE between erythrophores and xanthophores; in purple, DE between erythrophores and xanthophores; in brown, *pax7b*, encoding a transcription factor that promotes xanthophore development[S7] and expressed in both erythrophores and xanthophores. Despite harboring several genes of the BMP pathway, Chr23 was not enriched significantly for such genes compared to other chromosomes (Fisher's Exact test, P=0.7).

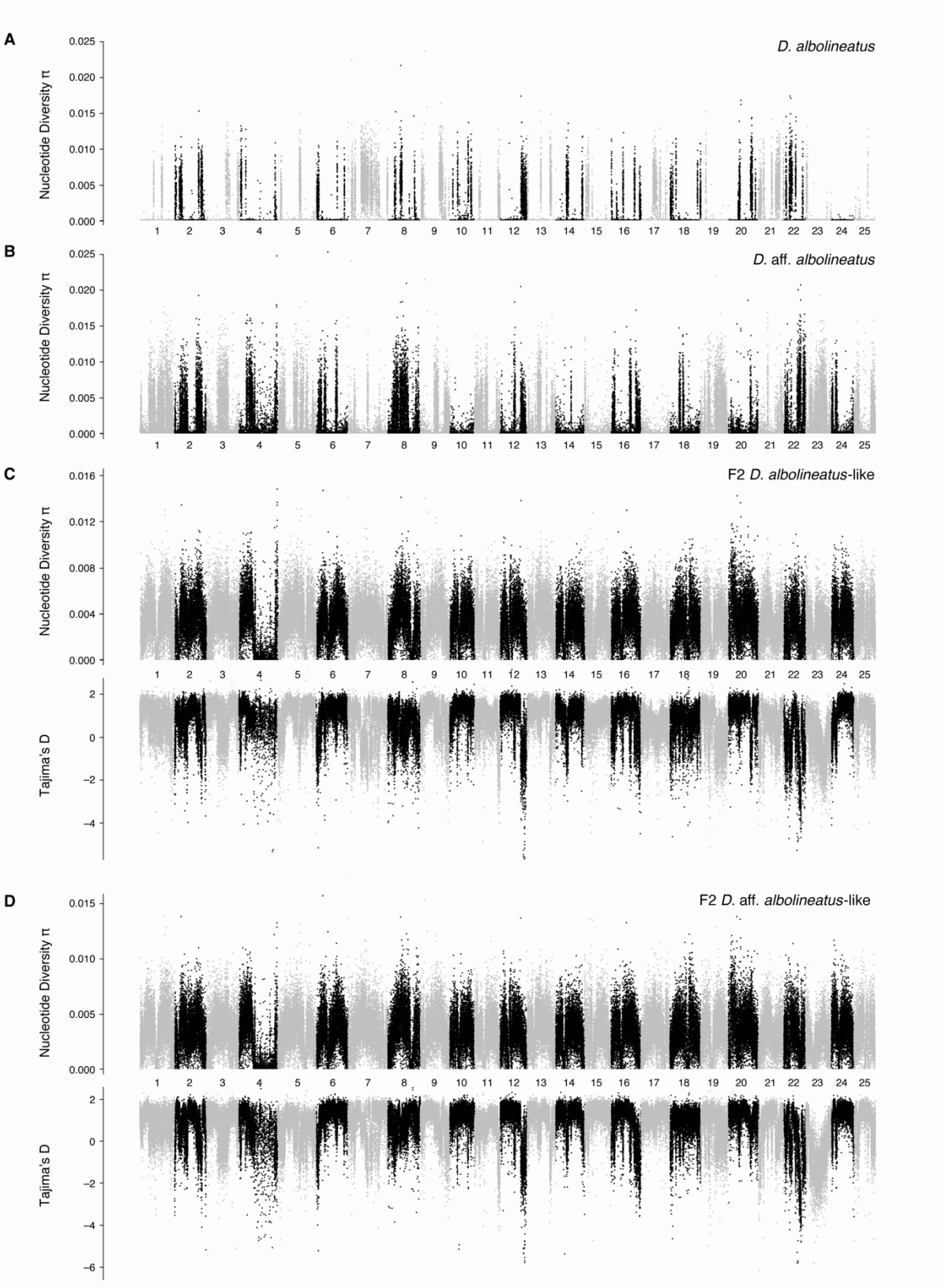
A
D. albolineatus
Nucleotide Diversity π
0.025
0.020
0.015
0.010
0.005
0.000
1 2 3 4 5 6 7 8 9 10 11 12 13 14 15 16 17 18 19 20 21 22 23 24 25
B
D. aff. albolineatus
Nucleotide Diversity π
0.025
0.020
0.015
0.010
0.005
0.000
1 2 3 4 5 6 7 8 9 10 11 12 13 14 15 16 17 18 19 20 21 22 23 24 25
C
F2 D. albolineatus-like
Nucleotide Diversity π
0.016
0.012
0.008
0.004
0.000
1 2 3 4 5 6 7 8 9 10 11 12 13 14 15 16 17 18 19 20 21 22 23 24 25
Tajima's D
2
0
−2
−4
D
F2 D. aff. albolineatus-like
Nucleotide Diversity π
0.015
0.010
0.005
0.000
1 2 3 4 5 6 7 8 9 10 11 12 13 14 15 16 17 18 19 20 21 22 23 24 25
Tajima's D
2
0
−2
−4
−6

Figure S8. Patterns of allelic variation across parental and pooled genomes of F2 fish. Related to Figure 4.

(A) Nucleotide diversity (π) of the parental *D. albolineatus* (female) indicated relatively low levels of genetic diversity across the genome consistent with a high degree of inbreeding since 1995 when fish were collected in the wild.

(B) Higher levels of nucleotide diversity were evident for the *D.* aff. *albolineatus* (male) parent; these fish were derived from the pet trade ("pink pearl danio") ca. 2003[S8].

(C,D) Nucleotide diversity and Tajima's D for fish of the *D. albolineatus*-like pool (C) and *D*. aff. *albolineatus*-like pool (D). Abundant nucleotide diversity, and greater than that for D. albolineatus alone, confirms segregation of grandparental alleles and indicates that peaks of association do not merely represent failures of segregation or sequencing artifacts. Negative values of Tajima's D indicate an abundance of rare alleles, as may occur with directional selection followed by rapid population expansion; high values indicate a scarcity of rare alleles, as can occur under conditions of balancing selection or sudden reductions in population size[S9]. Note the comparatively lower values of Tajima's D throughout Chr23, as well as candidate regions on Chr17.

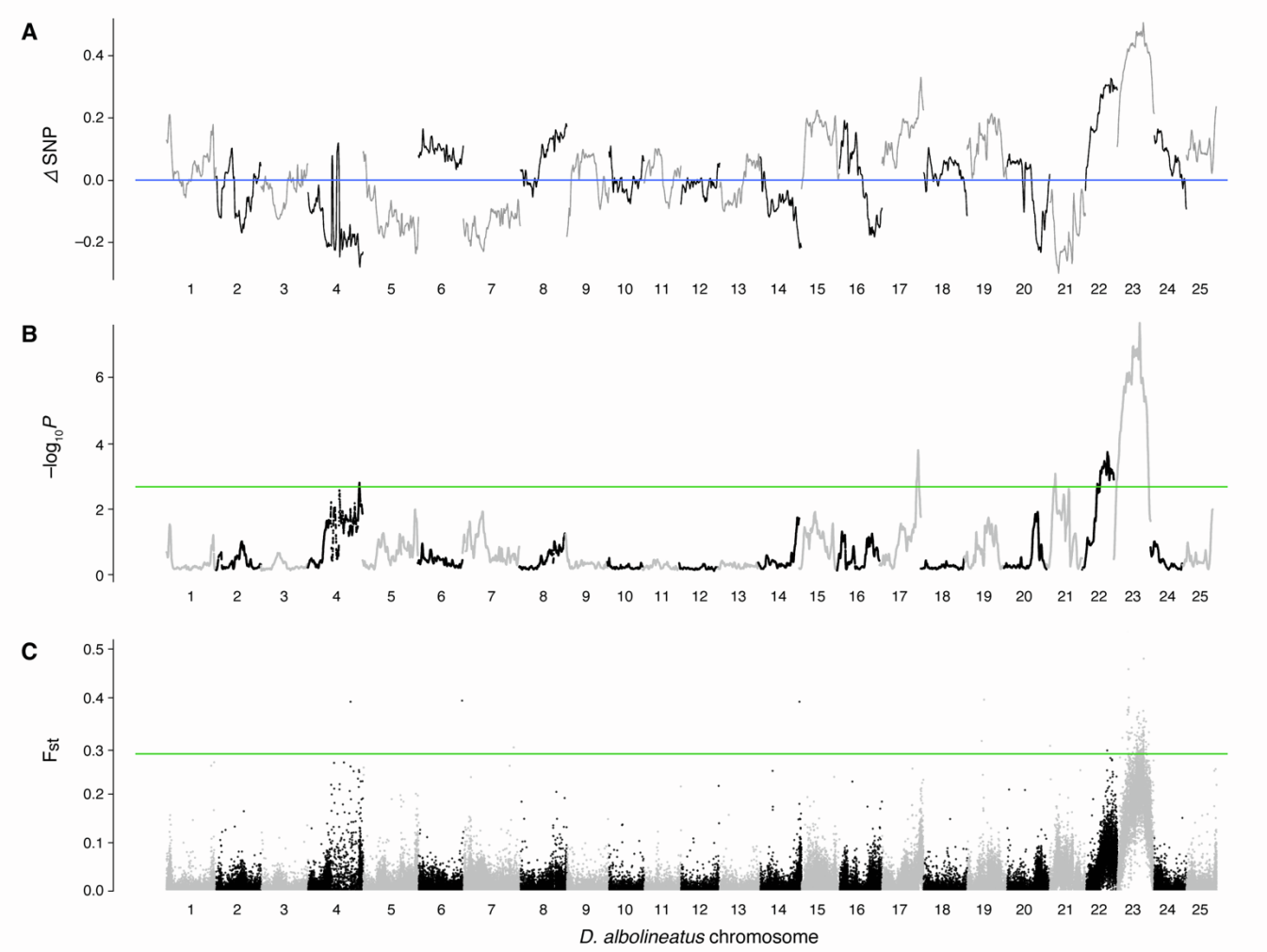

Figure S9. Genome-wide variation associated with phenotypes resembling *D. albolineaus* and *D.* aff. *albolineatus* in pooled sequencing of F2 fish. Related to Figure 4.

(A) Phased ΔSNP, where the Y axis represents a difference in proportion of the *D. albolineatus* alleles in the *D. albolineatus*-like and *D*. aff. *albolineatus*-like pools (Figure S8B), with positive values indicating an excess of *D. albolineatus* alleles in the *D. albolineatus*-like pool. A value of 0 (blue line) indicates regions in which the frequency of *D. albolineatus* alleles equals that of *D*. aff. *albolineatus* alleles in the *D. albolineatus*-like pool; a value of 1 would indicate regions in which the *D. albolineatus*-like pool is fixed for *D. albolineatus* alleles, whereas the *D*. aff. *albolineatus*-like pool would be depleted of them, with only *D*. aff. *albolineatus* alleles.

(B) Associations between pool phenotypes and allele frequencies, with kernel smoothed $-\log_{10}$(p-values; same plot as in Figure 4B, shown here for comparison with other metrics). Green line, q=0.01.

(C) F_{st} statistics between *D. albolineatus*-like and *D*. aff. *albolineatus*-like pools calculated with grenedalf using haploid population sizes of n=46 (2x sample size within each pool). Green line, top 0.1 percentile of F_{st} values.

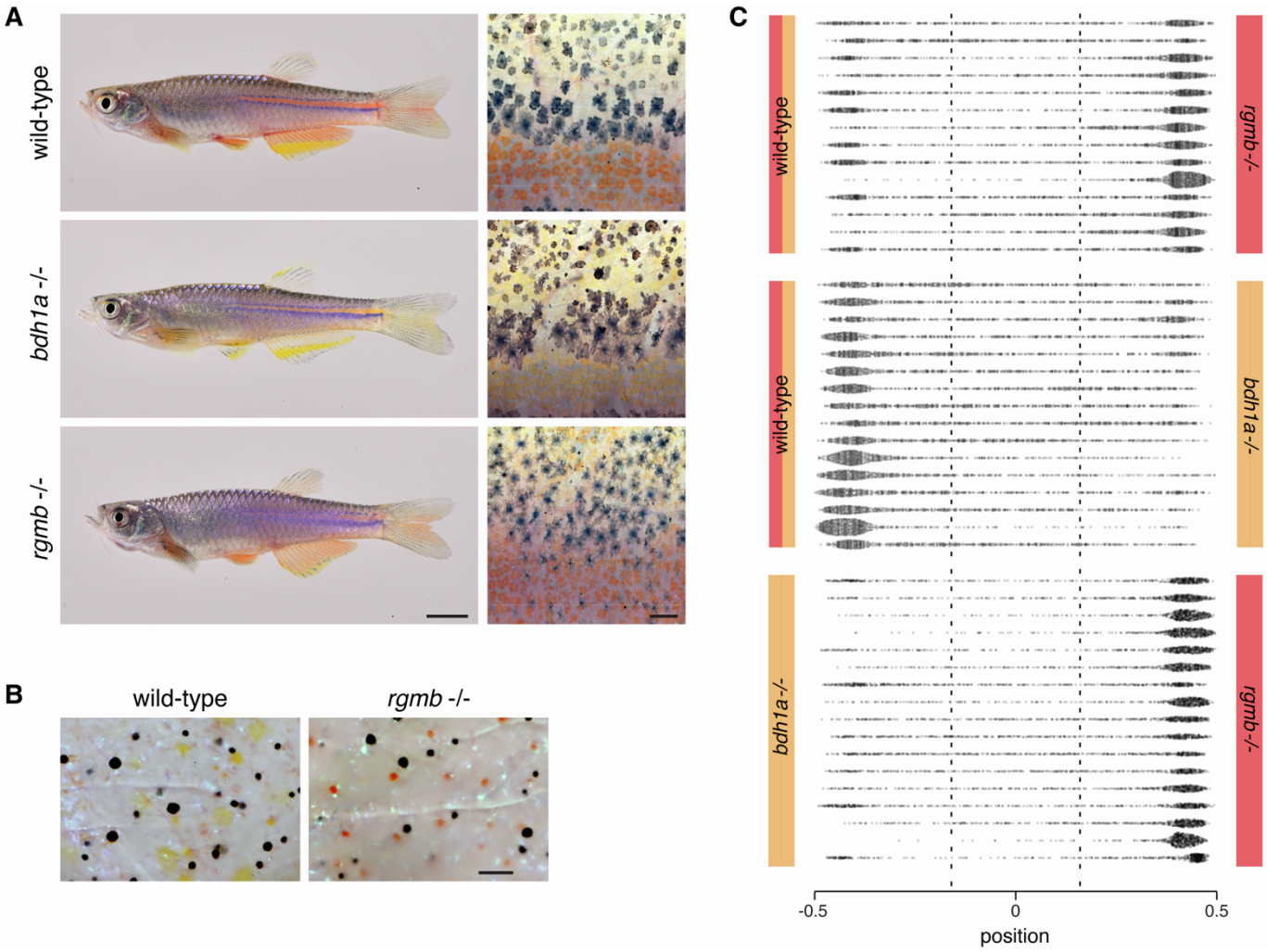

Figure S10. Red-deficient and super-red phenotypes provide opposing signals for shoaling. Related to Figure 4.

(A) Whole-fish phenotypes and flank closeups of wild-type, *bdh1a* and *rgmb* mutants. Higher magnification views at right illustrate patterns and color differences in the vicinity of a residual dorsal melanophore stripe in wild-type (darker melanophores). Ventral to this stripe are cells of the interstripe, comprising erythrophores and deeper iridophores that appear as a blue-tinted matte of cells in this image. Dorsal to the stripe are lighter melanophores interspersed with xanthophores. In *bdh1a-/-*, yellow cells occur both within the interstripe and dorsally. In *rgmb-/-*, erythrophores of the interstripe are more numerous, melanophores are more dispersed and lighter in color, and reddish erythrophores are found in place of xanthophores dorsally.

(B) Body pigment cells at dorsal scales of wild-type and *rgmb* mutant following epinephrine treatment, showing differences in pigment color.

(C) Positions of individual female fish relative to stimulus males as determined at 0.5 sec (15 video fame) intervals. Each row is a different individual; actual sides used for stimulus shoals were alternated betweem trials. Vertical dashed lines demarcate thirds of each tank with preference areas defined for each stimulus shoal at left and right (differences in total times spent between areas are shown in Figure 4C).

Scale bars, 5 mm (A, left), 200 μm (A, right), 100 μm (B).

Supplemental References

S1. Huang, D., Lewis, V.M., Foster, T.N., Toomey, M.B., Corbo, J.C., and Parichy, D.M. (2021). Development and genetics of red coloration in the zebrafish relative Danio albolineatus. eLife *10*. 10.7554/eLife.70253.

S2. Mills, M.G., Nuckels, R.J., and Parichy, D.M. (2007). Deconstructing evolution of adult phenotypes: genetic analyses of kit reveal homology and evolutionary novelty during adult pigment pattern development of Danio fishes. Development *134*, 1081‐1090. 10.1242/dev.02799.

S3. Parichy, D.M., Rawls, J.F., Pratt, S.J., Whitfield, T.T., and Johnson, S.L. (1999). Zebrafish sparse corresponds to an orthologue of c-kit and is required for the morphogenesis of a subpopulation of melanocytes, but is not essential for hematopoiesis or primordial germ cell development. Development *126*, 3425‐3436.

S4. Gur, D., Bain, E.J., Johnson, K.R., Aman, A.J., Pasoili, H.A., Flynn, J.D., Allen, M.C., Deheyn, D.D., Lee, J.C., Lippincott-Schwartz, J., and Parichy, D.M. (2020). In situ differentiation of iridophore crystallotypes underlies zebrafish stripe patterning. Nat Commun *11*, 6391. 10.1038/s41467-020-20088-1.

S5. Huang, D., Kapadia, E.H., Liang, Y., Shriver, L.P., Dai, S., Patti, G.J., Humbel, B.M., Laudet, V., and Parichy, D.M. (2025). Agouti and BMP signaling drive a naturally occurring fate conversion of melanophores to leucophores in zebrafish. Proc Natl Acad Sci U S A *122*, e2424180122. 10.1073/pnas.2424180122.

S6. Huang, D., Liu, T., Carr, A.A., de Mello, P.H., Liang, Y., Shriver, L.P., Chauvigne, F., Johnson, S.L., Cerda, J., Patti, G.J., and Parichy, D.M. (2025). Cell type diversification and phenotype convergence underlying white fin-ornamentation of cyprinid fishes. bioRxiv, 2025.2012.2026.696501. 10.64898/2025.12.26.696501.

S7. Nord, H., Dennhag, N., Muck, J., and von Hofsten, J. (2016). Pax7 is required for establishment of the xanthophore lineage in zebrafish embryos. Mol Biol Cell *27*, 1853‐1862. 10.1091/mbc.E15-12-0821.

S8. Quigley, I.K., Manuel, J.L., Roberts, R.A., Nuckels, R.J., Herrington, E.R., MacDonald, E.L., and Parichy, D.M. (2005). Evolutionary diversification of pigment pattern in Danio fishes: differential fms dependence and stripe loss in D. albolineatus. Development *132*, 89‐104. 10.1242/dev.01547.

S9. Tajima, F. (1989). Statistical method for testing the neutral mutation hypothesis by DNA polymorphism. Genetics *123*, 585‐595. 10.1093/genetics/123.3.585.

S10. Bröer S., Bröer A., Schneider H.P., Stegen C., Halestrap A.P., Deitmer J.W. Characterization of the high-affinity monocarboxylate transporter MCT2 in Xenopus laevis oocytes. Biochem. J. 1999;341:529–535. doi:10.1042/0264-6021:3410529.

S11. Shi Y., Chen D., Wang Y., Zhang C., Cao Y., Liu Y., Song T., Tan C., Peng Y. Filiform fire needling therapy relieves T cells-mediated melanocyte apoptosis and dysfunction by inhibiting JAK/STAT3 pathway via Mfsd4a in vitiligo. Chin. Med. 2025;20:117. doi:10.1186/s13020-025-01172-4.

S12. Yang Y., Luo Z., Hao Y., Ba W., Wang R., Wang W., Ding X., Li C. mTOR-mediated Na+/Ca2+ exchange affects cell proliferation and metastasis of melanoma cells. Biomed. Pharmacother. 2017;92:744–749. doi:10.1016/j.biopha.2017.05.104.

S13. Meng Y., Guo D., Lin L., Zhao H., Xu W., Luo S., Jiang X., Li S., He X., Zhu R., et al. Glycolytic enzyme PFKL governs lipolysis by promoting lipid droplet-mitochondria tethering to enhance beta-oxidation and tumor cell proliferation. Nat. Metab. 2024;6:1092–1107. doi:10.1038/s42255-024-01047-2.